SUCNR1 controls an anti-inflammatory program in macrophages to regulate metabolic response to obesity

Noelia Keiran[a,b,*], Victoria Ceperuelo-Mallafré[a,b,*], Enrique Calvo[a,b], Maria Isabel Hernández-Alvarez[a,b,c] Miriam Ejarque[a,b], Catalina Núñez-Roa[a,b], Daniel Horrillo[d], Elsa Maymó-Masip[a,b], M. Mar Rodríguez[a,b], Rosa Fradera[e], Juan Vladimir de la Rosa[f,g], Rosa Jorba[h], Ana Megia[a,b], Antonio Zorzano[b,c,i], Gema Medina-Gómez[d], Carolina Serena[a,b], Antonio Castrillo[f,g], Joan Vendrell[a,b,j#], Sonia Fernández-Veledo[a,b,#]

[a] Unitat de Recerca. Hospital Universitari de Tarragona Joan XXIII. Institut d´Investigació Sanitària Pere Virgili. Tarragona, Spain

[b] CIBER de Diabetes y Enfermedades Metabólicas Asociadas (CIBERDEM), Instituto de Salud Carlos III, Madrid, Spain

[c] Institute for Research in Biomedicine (IRB Barcelona). The Barcelona Institute of Science and Technology, Barcelona, Spain

[d] Departamento de Ciencias Básicas de la Salud, Área de Bioquímica y Biología Molecular. Universidad Rey Juan Carlos. Alcorcón, Madrid, Spain

[e] General and Digestive Surgery Service. Hospital St. Pau i Sta Tecla. Institut d´Investigació Sanitària Pere Virgili. Tarragona, Spain

[f] Instituto de Investigaciones Biomédicas "Alberto Sols" CSIC-UAM. Madrid. Spain

[g] Unidad de Biomedicina (Unidad Asociada al CSIC), Instituto Universitario de Investigaciones Biomédicas y Sanitaria (IUBIS), Universidad de Las Palmas de Gran Canaria, Las Palmas, Spain

[h] General and Digestive Surgery Service. Hospital Universitari de Tarragona Joan XXIII. Institut d´Investigació Sanitària Pere Virgili. Tarragona, Spain

[i] Departament de Bioquímica i Biomedicina Molecular, Facultat de Biología. Barcelona, Spain

[j]Universitat Rovira i Virgili, Tarragona, Spain

* Equally contributed

#co-corresponding and senior authors: J Vendrell or S Fernández-Veledo, Unitat de Recerca. Hospital Universitari de Tarragona Joan XXIII. Institut d´Investigació Sanitària Pere Virgili, c/o Dr Mallafré Guasch, 4, Tarragona 43007, Spain. Tel: +34 977 29 58 00 Ext 3401; Fax: +34 977 29 58 23; E-mail: jvo@comt.es or sonia.fernandezveledo@gmail.com

Keywords: immunometabolism, succinate, macrophages, inflammation, obesity, SUCNR1

ABSTRACT

Succinate is a signaling metabolite sensed extracellularly by SUNCR1. Succinate accumulation in macrophages is known to activate a pro-inflammatory program; however, the contribution of SUCNR1 to macrophage phenotype and function has remained unclear. Here, we found that activation of SUCNR1 had a critical role in the anti-inflammatory responses in macrophages. Myeloid-specific deficiency in SUCNR1 promoted a local pro-inflammatory phenotype, disrupted glucose homeostasis in mice fed a normal chow diet, exacerbated the metabolic consequences of diet-induced obesity and impaired adipose tissue browning in response to cold exposure. Activation of SUCNR1 promoted an anti-inflammatory phenotype in macrophages and boosted the response of these cells to type 2 cytokines, including IL-4. Succinate decreased the expression of inflammatory markers in adipose tissue from lean, but not obese subjects, who had lower expression of SUCNR1 in adipose tissue-resident macrophages. Our findings highlight the importance of succinate–SUCNR1 signaling in determining macrophage polarization and assign a role to succinate in limiting inflammation.

Traditionally considered an energetic metabolite of the mitochondrial tricarboxylic acid cycle, succinate has recently emerged as a metabolic signal governing local stress, tissue damage and immunologic danger[1, 2, 3, 4]. Thus, in certain activated innate immune cells or in cells relying on anaerobic glycolysis in hypoxia, the amount of mitochondrial succinate increases[5] and is then released into the cytosol where its accumulation is directly related to protein succinylation, stabilization of the transcription factor HIF-1α, epigenetic regulation and ROS production[1, 3, 5].

Succinate can also be released to the extracellular space through plasma membrane transporters of the SLC13 family, by poorly understood processes[4, 6]. Elevated amounts of circulting succinate occur in some physiological conditions, such as endurance exercise[7] and in certain pathologies, including hypertension[8], ischemic heart disease[9], type 2 diabetes mellitus[8, 10] and obesity[8, 11]. Extracellular succinate binds its receptor SUCNR1 (or GPR91)[12] on the plasma membrane of a broad range of cells[13, 14]. To date, activation of SUCNR1 by extracellular succinate has been associated with pathological cardiomyocyte hypertrophy[9], normal retinal development and proliferative ischemic retinopathy[15], pathogenesis of diabetic nephropathy by activating renin-angiotensin system[4, 6, 16], hepatic fibrosis through activation of α-SMA production in stellate cells[17] and adipose tissue expansion *via* SUCNR1-dependent antilipolytic effects in adipocytes[18], among others.

The succinate-SUCNR1 signaling axis has a complex role in immune responses[19, 20]. Dendritic cells (DCs) sense immunological danger through SUCNR1, to enhance antigen-presenting functions required for optimal immune activation[2, 21]. Further, the absence of SUCNR1 produces a hyperactive mast cell phenotype[22]. While succinate is known to be released by lipopolysaccharide (LPS)-activated pro-inflammatory macrophages[23], the role of SUCNR1 in macrophage plasticity remains largely unknown. Thus, despite early reports that SUCNR1 activation boosts pro-inflammatory responses in macrophages during antigen-induced arthritis[23], SUCNR1-deficient peritoneal macrophages have a similar cytokine profile as those derived from wild-type animals, both in basal and in LPS-stimulated conditions[10]. Moreover, recent reports showed that extracellular succinate might also mediate anti-inflammatory responses in neural stem cells[24] Indeed,

SUCNR1 has been described as a major driver of microbiota-triggered type 2 immunity in intestine[25].

There is strong evidence that succinate-SUCNR1 signaling serves as a link between metabolic stress and inflammation; however, whether succinate can be regarded as a harmful signal or has a protective role remains controversial. Because obesity is associated with chronic inflammation, and because macrophages are central mediators in obesity-associated inflammation, here we used mice with conditional inactivation of *Sucnr1* in myeloid cells to investigate the role of succinate-SUCNR1 signaling in obesity. We found that SUCNR1 modulated the phenotype of bone marrow-derived macrophages (BMDM) in a cell-autonomous manner. SUCNR1 signaling induced an anti-inflammatory phenotype in adipose tissue-resident macrophages (ATMs) and dampened tissue inflammation both at steady-state and after challenges that disrupted metabolic homeostasis. Our data strengthen the idea that macrophages have a key role in the pathogenesis of obesity and identify succinate-SUCNR1 signaling as a metabolic guardian in inflammatory-associated disorders.

RESULTS

Myeloid *Sucnr1* deficiency provokes inflammation and glucose intolerance

To elucidate the role of succinate-SUCNR1 signaling in macrophages, we crossed mice bearing a conditional loxP-flanked ("floxed") allele of *Sucnr1* (*Sucnr1*$^{fl/fl}$, used as control mice) to transgenic mice expressing bacterial Cre recombinase under the control of the lysozyme 2 promoter (*LysM*-Cre) to generate mice with myeloid cell-specific *Sucnr1* deficiency (hereafter referred to as *LysM*-Cre *Sucnr1*$^{fl/fl}$) (Supplementary Fig. 1). *LysM*-Cre *Sucnr1*$^{fl/fl}$ mice were born in a Mendelian ratio, and no obvious morphological differences were observed between genotypes (data not shown). Gene analysis showed that expression of *Sucnr1* mRNA was negligible in BMDMs, elicited-peritoneal macrophages (pMs) and adipose-tissue resident macrophages (ATMs) from *LysM*-Cre *Sucnr1*$^{fl/fl}$ mice (Fig. 1a). No significant differences were found between *LysM*-Cre *Sucnr1*$^{fl/fl}$ and *Sucnr1*$^{fl/fl}$ mice in body and fat-pad weight (Fig. 1b,c; Supplementary Fig. 2a) and energy metabolic parameters measured by indirect calorimetry (Supplementary Fig. 2b,c) when they were fed a normal chow diet (NCD) for 20 weeks. Serum glucose was also comparable between genotypes (Fig. 1c); however, insulin levels were higher in *LysM*-Cre *Sucnr1*$^{fl/fl}$ mice (Fig. 1c), and they also exhibited impaired glucose tolerance (Fig. 1d) and insulin sensitivity (Fig. 1e) as compared with *Sucnr1*$^{fl/fl}$ mice. Next, we evaluated the inflammatory status of white adipose tissue (WAT) and liver in *LysM*-Cre *Sucnr1*$^{fl/fl}$ and *Sucnr1*$^{fl/fl}$ mice. Gene analysis showed that the expression of genes typically linked to the development of insulin resistance, *Il1b*, *Il6*, *Il12b*, *Tnf* and *Nos2*, was higher in the subcutaneous (sc) and visceral (v) WAT and liver in *LysM*-Cre *Sucnr1*$^{fl/fl}$ mice than in *Sucnr1*$^{fl/fl}$ mice (Fig. 1f), whereas *Arg1, Mrc1, Fizz1, Il10*, *Il4ra, Il1rn* were downregulated, particularly in the scWAT (Fig. 1g).

We next assessed the timing of glucose intolerance and insulin sensitivity in *LysM*-Cre *Sucnr1*$^{fl/fl}$ mice. Insulin resistance, but not glucose intolerance, was detected in 15-week-old *LysM*-Cre *Sucnr1*$^{fl/fl}$ mice, but not in *Sucnr1*$^{fl/fl}$ mice (Supplementary Fig. 2d). WAT and liver inflammation, as assessed by expression of pro-inflammatory genes (*Il1b*, *Il6*, *Il12b*, *Tnf* and *Nos2)*, was manifest at 12-weeks of age in *LysM*-Cre *Sucnr1*$^{fl/fl}$ mice (Supplementary Fig. 2e), at a time when glucose tolerance and insulin sensitivity were

still similar to *Sucnr1*$^{fl/fl}$ control mice (Supplementary Fig. 2d), suggesting that in this model inflammation precedes the induction of insulin resistance.

Mirroring the increase in adipose tissue inflammation, the number of CD11b^{+}F4/80^{+} macrophages in the stromal vascular fraction (SVF) of scWAT and vWAT (refered to ATMs hereafter) was significantly higher in *LysM*-Cre *Sucnr1*$^{fl/fl}$ than in *Sucnr1*$^{fl/fl}$ mice, as measured by flow cytometry (Fig. 1h). The percentage of SVF CD11b^{+} myeloid cells in the scWAT and vWAT were similar in *LysM*-Cre *Sucnr1*$^{fl/fl}$ and *Sucnr1*$^{fl/fl}$ mice (Supplementary Fig. 2f) and there were no significant differences in the number of CD11b^{+}Ly6G^{+} neutrophils (Supplementary Fig. 2g). Sorting of CD11b^{+}CD11c^{+}CD206^{-} pro-inflammatory macrophages and CD11b^{+}CD11c^{-}CD206^{+} anti-inflammatory macrophages[26] from the scWAT indicated a significant increase in the percentage of CD11b^{+}CD11c^{+}CD206^{-} macrophages in *LysM*-Cre *Sucnr1*$^{fl/fl}$ (25.9%) compared with *Sucnr1*$^{fl/fl}$ mice (18.8%), concomitant with a decrease in the percentage of CD11b^{+}CD11c^{-}CD206^{+} macrophages (0.8%) in *LysM*-Cre *Sucnr1*$^{fl/fl}$ mice compared with *Sucnr1*$^{fl/fl}$ mice (1.3%; Supplementary Fig. 2h). In addition, immunoblot analysis of mitogen-activated protein kinase JNK phosphorylation in adipose tissue[27] indicated JNK activation in the scWAT and vWAT of *LysM*-Cre *Sucnr1*$^{fl/fl}$ mice relative to *Sucnr1*$^{fl/fl}$ mice (Fig. 1i). These results suggested that myeloid-specific deficiency of *Sucnr1* promoted an overt pro-inflammatory response and disrupted glucose homeostasis during steady-state.

Myeloid *Sucnr1* deficiency exacerbates diet-induced obesity

We next assessed the susceptibility of *LysM*-Cre *Sucnr1*$^{fl/fl}$ mice to high-fat diet (HFD)-induced obesity. Body weight gain was significantly increased in HFD *LysM*-Cre *Sucnr1*$^{fl/fl}$ mice relative to HFD *Sucnr1*$^{fl/fl}$ mice (Fig. 2a and Supplementary Fig. 3a), which correlated with a significant increase in the mass of the WAT, pancreas and liver (Supplementary Fig. 3b). Plasma levels of succinate were significantly higher in *LysM*-Cre *Sucnr1*$^{fl/fl}$ mice than in *Sucnr1*$^{fl/fl}$ mice (Fig. 2b). Also, intracellular succinate was higher in WAT (Supplementary Fig. 3.c), adipocytes and ATMs isolated from fat depots (Supplementary Fig. 3d) of *LysM*-Cre *Sucnr1*$^{fl/fl}$ than of *Sucnr1*$^{fl/fl}$ mice. Expression of *Sucnr1* mRNA in scWAT was higher in HFD *LysM*-Cre *Sucnr1*$^{fl/fl}$ and HFD *Sucnr1*$^{fl/fl}$ mice than in NCD mice of both genotypes (Fig. 2b), whereas HFD decreased the expression of *Sucnr1* mRNA in ATMs from scWAT of *Sucnr1*$^{fl/fl}$ mice (Fig. 2b). This

suggested that the increased expression of *Sucnr1* mRNA in the scWAT in HFD *LysM*-Cre *Sucnr1*$^{fl/fl}$ and *Sucnr1*$^{fl/fl}$ mice originated from mature adipocytes.

The size of adipocytes in the scWAT of HFD *LysM*-Cre *Sucnr1*$^{fl/fl}$ mice was significantly increased compared with *Sucnr1*$^{fl/fl}$ mice (Supplementary Fig. 3e). There was also an increase in the number of crown-like structures in the scWAT and vWAT of HFD *LysM*-Cre *Sucnr1*$^{fl/fl}$ mice compared with control mice (Fig. 2c). Of note, the increased weight gain in HFD *LysM*-Cre *Sucnr1*$^{fl/fl}$ mice was not associated with changes in food intake compared with HFD *Sucnr1*$^{fl/fl}$ mice (Supplementary Fig. 3f). Indirect calorimetry showed similar oxygen consumption and carbon dioxide production in both genotypes (Supplementary Fig. 3g). Likewise, there were no significant differences in energy expenditure (EE) (Figure 2.d). When the data were corrected to body weight, analysis of covariance[28] indicated that the differences detected in EE were genotype dependent (Supplementary Fig. 3h). The lower respiratory exchange ratio (VCO_2/VO_2) in HFD *LysM*-Cre *Sucnr1*$^{fl/fl}$ compared to HFD *Sucnr1*$^{fl/fl}$ mice (Fig. 2d) indicated a preference in these mice to metabolize fat as energy[29].

HFD *LysM*-Cre *Sucnr1*$^{fl/fl}$ mice had a higher fasting hyperglycemia and hyperinsulinemia than HFD *Sucnr1*$^{fl/fl}$ mice (Fig. 2e). Consistently, HFD *LysM*-Cre *Sucnr1*$^{fl/fl}$ mice showed impaired glucose tolerance (Fig. 2f) and insulin sensitivity (Fig. 2g) relative to HFD *Sucnr1*$^{fl/fl}$ mice. No significant differences in glucose tolerance and insulin sensitivity were detected between both genotypes before their body weight diverged (11–15 weeks of age) (Supplementary Fig. 3i), indicating that the loss of glucose homeostasis in HFD *LysM*-Cre *Sucnr1*$^{fl/fl}$ mice was linked to their obese phenotype. Further, no significant differences in oxygen consumption, carbon dioxide production and EE were detected between genotypes at 14 weeks of age (Supplementary Fig. 3j), indicating that, in response to dietary excess, the metabolic differences between both genotypes were mostly related to weight gain.

Similar to the findings on NCD, HFD *LysM*-Cre *Sucnr1*$^{fl/fl}$ mice showed higher expression of several pro-inflammatory markers (*Il12b*, *Tnf* and *Nos2*) in WAT and liver (Fig. 2h) and a decrease in the expression of some anti-inflammatory markers (*Arg1, Mrc1, Il10* and *Il4ra*) in scWAT (Fig. 2i) as compared with HFD *Sucnr1*$^{fl/fl}$ mice. We observed a higher frequency of $CD11b^{+}CD11c^{+}CD206^{-}$ pro-inflammatory macrophages

(23.8%), along with a trend for a lower frequency of $CD11b^{+}CD11c^{-}CD206^{+}$ anti-inflammatory macrophages (1.3%) in the scWAT of HFD *LysM*-Cre *Sucnr1*$^{fl/fl}$ compared with HFD *Sucnr1*$^{fl/fl}$ mice (19.3 and 3.1%, respectively) (Supplemmentary Fig. 3k). Taken together, the results indicate that myeloid-specific *Sucnr1* deficiency increases the susceptibility to diet-induced obesity.

***Sucnr1* signaling regulates cell-autonomous macrophage polarization**

To address whether intracellular and extracellular succinate had different effects on macrophages, first we investigated whether expression of *Sucnr1* mRNA was affected by the activation status of macrophages. As reported before[3, 23, 24], stimulation with LPS, but not IL-4, increased the secretion of succinate in pMS *in vitro* (Fig. 3a), and correlated with an accumulation of intracellular succinate (Supplementary Fig. 4a), as previously described[30]. Expression of *Sucnr1* mRNA in pMs was robustly increased by IL-4 and strongly decreased by LPS (Fig. 3a), while *SUCNR1* mRNA in the human monocyte-like cell line THP1 was induced by M-CSF and decreased by GM-CSF (Supplementary Fig. 4b). In macrophages differentiated with GM-CSF from human peripheral blood mononuclear cell (hPBMCs) succinate secretion was increased compared to non-differentiated (control) cells, whereas *SUNCR1* mRNA was increased in macrophages differentiated with M-CSF compared to control cells (Fig. 3b). Polarization of hPBMC macrophages by GM-CSF or M-CSF was confirmed by measuring the expression of pro-inflammatory-associated (*IL1β*, *IL6*, *IL12β*, *TNF* and *MCP1*) and anti-inflammatory-associated (*PPARγ* and *MRC1*) genes, respectively (Supplementary Fig. 4c)[31]. hPBMCs-derived M-CSF-differentiated macrophages (hereafter hPBMCs$^{M\text{-}CSF}$ macrophages) can be polarized towards a pro- or an anti-inflammatory phenotype with the appropriate exogenous stimuli[32]. LPS significantly decreased the expression of *SUCNR1* mRNA in hPBMCs$^{M\text{-}CSF}$ macrophages, whereas IL-4 strongly enhanced its expression (Fig. 3c). Accordingly, the expression of anti-inflammatory markers, such as *Arg1* and *Fizz1*, and fatty acid metabolic genes, such as *Cpt1a* and *Fasn*, was significantly lower in pMs isolated from LysM-Cre *Sucnr1*$^{fl/fl}$ compared with those isolated from *Sucnr1*$^{fl/fl}$ mice (Fig. 3d). We detected a lower expression of *Arg1* and *Mrc1* in IL-4-treated *LysM*-Cre *Sucnr1*$^{fl/fl}$ pMs compared to IL-4-treated *Sucnr1*$^{fl/fl}$ pMs (Fig. 3e). M-CSF-treated BMDMs (hereafter BMDMs$^{M\text{-}CSF}$) from *LysM*-Cre *Sucnr1*$^{fl/fl}$ mice also expressed less anti-inflammatory genes (*Arg1*, *Mrc1* and *Fizz1*) compared with *Sucnr1*$^{fl/fl}$ BMDMs$^{M\text{-}CSF}$ (Fig. 3f). M-CSF, but not GM-CSF, induced the expression of *Sucnr1* mRNA in BMDMs

(Supplementary Fig. 4d). Accordingly, succinate enhanced the expression *Arg1*, *Mrc1*, *Fizz1* and *IL10* in *Sucnr1*$^{fl/fl}$ BMDMs$^{M\text{-}CSF}$, but not in *LysM*-Cre *Sucnr1*$^{fl/fl}$ BMDMs$^{M\text{-}CSF}$ (Fig. 3g). Addition of succinate to *Sucnr1*$^{fl/fl}$ BMDMs$^{M\text{-}CSF}$ did not increase the amount of intracellular succinate, whereas the cell-permeable dimethyl succinate did (Supplementary Fig. 4e). There were no significant differences in the amount of intracellular succinate between *Sucnr1*$^{fl/fl}$ BMDMs and *LysM*-Cre *Sucnr1*$^{fl/fl}$ BMDMs (Supplementary Fig. 4f).

An *in silico* analysis of the *Sucnr1* promotor region in BMDMs revealed binding sites for the IL-4-responsive transcription factor STAT6 (Supplementary Fig. 5a). To test whether expression of SUCNR1 in macrophages was regulated by IL-4, we used small-interfering RNA to knock down the expression of STAT6 or KLF4, a transcription factor whose expression is induced by STAT6 in macrophages[33]. The IL-4-induced expression of *IL10*, *PPARG* and *IL1RN* (Supplementary Fig. 5b) and *SUCNR1* (Fig. 4a) was lower in THP-1 cells in which STAT6 or KLF4 were knocked down compared with control-siRNA THP-1 macrophages (65% or 68% efficiency of knock down, respectively). IL-4 stimulation upregulated *Sucnr1* (Fig. 4b) and *Arg1*, *Mrc1* and *Il10* mRNA (Supplementary Fig. 5c) in *Sucnr1*$^{fl/fl}$ BMDMs$^{M\text{-}CSF}$, but not in *Stat6*$^{-/-}$ BMDMs$^{M\text{-}CSF}$. Knock down of STAT6 and KLF4 also decreased the upregulation of *Sucnr1* (Fig. 4.c) and *Arg1*, *Mrc1* and *Il10* mRNA (Supplementary Fig. 5d) in response to IL-4 in *Sucnr1*$^{fl/fl}$ BMDMs$^{M\text{-}CSF}$. Knock down of KLF4 in BMDMs$^{M\text{-}CSF}$ also decreased the IL-4-induced expression of SUCNR1 protein (Fig. 4d), while IL-4 did not upregulate expression of KLF4 or SUCNR1 protein in *Stat6*$^{-/-}$ BMDMs$^{M\text{-}CSF}$ (Supplementary Fig. 5e).

The KLF4 promoter contains CREB binding sites[34] and can therefore be modulated by G protein-coupled receptor (GPCR) ligands, which can act synergically with IL-4 through the activation of the cAMP-CREB pathway[34, 35]. Consistent with this notion, short-term exposure of *Sucnr1*$^{fl/fl}$ BMDMs$^{M\text{-}CSF}$ to succinate induced the phosphorylation of PKA and CREB, which was blocked by the PKA inhibitor H-89 (Fig. 4e). The succinate-mediated activation of the PKA-CREB pathway was not detected in *LysM*-Cre *Sucnr1*$^{fl/fl}$ BMDMs$^{M\text{-}CSF}$ (Fig. 4f), while H-89-mediated inhibition of PKA or knockdown of *Klf4* by siRNA in *Sucnr1*$^{fl/fl}$ BMDMs$^{M\text{-}CSF}$ suppressed the induction of *Il10* and *Sucnr1* mRNA by succinate (Fig. 4g). Finally, we assessed the effect of succinate on IL-4 signaling. Whereas succinate treatment did not significantly modify the IL-4-induced activation of

STAT6 in *Sucnr1*$^{fl/fl}$ BMDMs$^{M\text{-}CSF}$ (Supplementary Fig. 5f), succinate increased the IL-4-induced activation of PKA and CREB in these cells, an effect that was absent in *LysM*-Cre *Sucnr1*$^{fl/fl}$ BMDMs$^{M\text{-}CSF}$ (Fig. 4h) and abolished by H-89 treatment (Fig. 4i). Succinate increased the IL-4-induced expression of KLF4 and IL-10 in *Sucnr1*$^{fl/fl}$ BMDMs$^{M\text{-}CSF}$, but not in *LysM*-Cre *Sucnr1*$^{fl/fl}$ BMDMs$^{M\text{-}CSF}$ (Fig. 4h), suggesting that succinate enhanced IL-4 signaling by modulating the activation of PKA and CREB and the expression of KLF4. Accordingly, addition of H-89 prevented the succinate-induced increase in *Il10* and *Arg1* mRNA in IL-4-treated BMDMs$^{M\text{-}CSF}$ (Fig. 4j). Overall, these data indicated that succinate-SUCNR1 signaling promoted an anti-inflammatory phenotype in macrophages.

Sucnr1 deficiency alters intracellular signaling in ATMs

Because ATMs play key roles in obesity-induced inflammation[36], we performed transcriptomic analysis on ATMs sorted from the scWAT and vWAT of *LysM*-Cre *Sucnr1*$^{fl/fl}$ and *Sucnr1*$^{fl/fl}$ mice. 242 genes (85 upregulated, 157 downregulated) were differentially expressed in scWAT ATMs, and 271 genes (174 up, 97 down) were differentially expressed in vWAT ATMs (FC>2, adj. pval<0.05) from *LysM*-Cre *Sucnr1*$^{fl/fl}$ mice compared to *Sucnr1*$^{fl/fl}$ mice (Fig. 5a). Gene set enrichment analysis (GSEA) indicated that loss of *Sucnr1* resulted in altered gene expression patterns in vWAT ATMs compared to scWAT ATMs (Fig. 5b). Specifically, inflammatory pathways such as interferon, epithelial mesenchymal transition and TNF response were upregulated in *LysM*-Cre *Sucnr1*$^{fl/fl}$ compared to *Sucnr1*$^{fl/fl}$ scWAT ATMs, while they were down regulated in *LysM*-Cre *Sucnr1*$^{fl/fl}$ compared to *Sucnr1*$^{fl/fl}$ vWAT ATMs vWAT ATMs (Fig. 5c). The opposite outcomes of *Sucnr1* deficiency in the transcriptional signature of ATMs (Fig. 5c, Supplementary Fig. 6a,b) were associated to the pro-inflammatory profile of *Sucnr1*$^{fl/fl}$ vWAT ATMs compared to *Sucnr1*$^{fl/fl}$ scWAT ATMs (Supplementary Fig. 6a,b), previously described in vWAT compared to scWAT[37]. GSEA analysis of the genes differentially regulated between scWAT ATMs and vWAT ATMs indicated the upregulation of inflammatory pathways in *LysM*-Cre *Sucnr1*$^{fl/fl}$ vWAT ATMs compared to *LysM*-Cre *Sucnr1*$^{fl/fl}$ scWAT ATMs (Supplementary Fig. 7a,b; Supplementary Table 1 and 2). Independent validation by qPCR indicated increased expression of *Il1β*, *Il6* and *Tnf* and decreased expression of *Il10* in *LysM*-Cre *Sucnr1*$^{fl/fl}$ scWAT ATMs compared with *Sucnr1*$^{fl/fl}$ scWAT ATMs (Fig. 5d). A decrease in *Tnf* and *Il10* mRNA was observed in *LysM*-Cre *Sucnr1*$^{fl/fl}$ vWAT ATMs compared with *Sucnr1*$^{fl/fl}$

vWAT ATMs (Fig. 5d). Both $CD11b^{+}CD11c^{+}CD206^{-}$ pro-inflammatory and $CD11b^{+}CD11c^{-}CD206^{+}$ anti-inflammatory macrophages from the *LysM*-Cre *Sucnr1*$^{fl/fl}$ scWAT (but not the vWAT) showed increased expression of pro-inflammatory genes compared with $CD11b^{+}CD11c^{+}CD206^{-}$ and $CD11b^{+}CD11c^{-}CD206^{+}$ macrophages from *Sucnr1*$^{fl/fl}$ mice (Fig. 5e,f).

The IL-4- and succinate-induced expression of anti-inflammatory markers (*Arg1*, *Mrc1*, *Fizz1* and *Il1rn*) was lower in *LysM*-Cre *Sucnr1*$^{fl/fl}$ than in *Sucnr1*$^{fl/fl}$ scWAT ATMs, both in cells isolated from mice fed a NCD or HFD (Fig. 6a,b). By contrast, LPS-induction of *Il1b* mRNA was higher in *LysM*-Cre *Sucnr1*$^{fl/fl}$ than in *Sucnr1*$^{fl/fl}$ scWAT ATMs, both in cells isolated from mice fed a NCD or HFD (Fig. 6c). Moreover, the succinate-induced expression of *Il10* and *Sucnr1* was blocked by inhibition of PKA (Fig. 6d) or knockdown of KLF4 (Fig. 6e) in scWAT ATMs from *Sucnr1*$^{fl/fl}$ mice. Thus, signaling through SUCNR1 had both inflammatory[23] and anti-inflammatory effects in ATMs, and succinate regulated an anti-inflammatory program in scATMs.

Myeloid Sucnr1 deficiency impairs cold-induced browning of scWAT

Type 2 immune signaling regulates adipose thermogenesis[38, 39, 40]. Next, we investigated whether succinate-SUCNR1 signaling in macrophages was involved in beige cell activation in the scWAT and cold-induced thermogenesis. Prolonged cold exposure (8ºC for 6 days) led to a marked induction of *Ucp1* and other key thermogenic genes in the scWAT of *Sucnr1*$^{fl/fl}$ mice, but only to poor induction in the scWAT of *LysM*-Cre *Sucnr1*$^{fl/fl}$ mice (Fig. 7a). Immunohistochemical analysis of scWAT indicated the formation of multilocular, brown-like adipocytes in *Sucnr1*$^{fl/fl}$ mice following cold exposure, but this effect was noticeably reduced in *LysM*-Cre *Sucnr1*$^{fl/fl}$ mice (Fig. 7b). Immunoblotting indicted a marked impairment in the cold-induced expression of Ucp1 protein in the scWAT of *LysM*-Cre *Sucnr1*$^{fl/fl}$ compared with *Sucnr1*$^{fl/fl}$ mice (Fig. 7c). However, the interscapular brown adipose tissue (BAT) of *LysM*-Cre *Sucnr1*$^{fl/fl}$ mice had higher Ucp1 expression, both mRNA (Fig. 7d) and protein (Fig. 7e), following prolonged cold exposure compared with the interscapular BAT of *Sucnr1*$^{fl/fl}$ mice. No significant differences were detected in EE or whole-body oxygen consumption in *LysM*-Cre *Sucnr1*$^{fl/fl}$ and *Sucnr1*$^{fl/fl}$ mice housed at ambient temperature (22ºC), thermoneutrality (30ºC) or prolonged cold-exposure (Fig. 7f). These results indicate that loss of Sucnr1 in myeloid cells limited the browning of scWAT, which is considered a type 2 immune

response[40].

Obesity disturbs succinate-SUCNR1 signaling in human adipose tissue

Circulating levels of succinate are higher in obese than in lean humans[11]. To determine whether obesity impacts SUCNR1 function in human adipose tissues, we analyzed its expression in scWAT and vWAT biopsies from people classified according to body-mass index (Supplementary Table 3). Circulating levels of succinate were higher in obese subjects than in lean controls (Supplementary Table 3)[11]. Further, expression of *SUCNR1* mRNA was higher in WAT from obese subjects than from lean ones, particularly in scWAT (Fig. 8a). Notably, we found a positive association between expression of *SUCNR1* in scWAT and clinical parameters associated with an altered metabolic profile such as blood glucose, hip circumference and diastolic blood pressure (Fig. 8b). Cellular fractionation of scWAT biopsies indicated increased expression of *SUCNR1* in mature adipocytes in obese subjects compared with lean (Fig. 8c), whereas the opposite was seen in scWAT ATMs (Fig. 8d). The decrease in *SUCNR1* mRNA in scWAT ATMs from obese compared with lean subjects correlated with lower *PPARG* and *MRC1* mRNA expression and was concomitant with higher expression of the pro-inflammatory genes *IL1B*, *TNF* and *MCP1* (Fig. 8e). To examine the effects of extracellular succinate in the adipose tissue with respect to inflammation, we incubated WAT explants obtained from lean and obese subjects with succinate for 24 h. Incubation of lean-derived scWAT with succinate significantly decreased the expression of the pro-inflammatory cytokines *IL1β*, *TNF* and *IL12B* compared with non-stimulated scWAT (Fig. 8f). By contrast, succinate increased mRNA expression of *IL1B*, *TNF* and *IL12B* in vWAT compared to non-stimulated vWAT (Fig. 8g). These observations suggest that succinate-SUCNR1 signaling had an anti-inflammatory role in the human scWAT, which was disturbed in obesity.

DISCUSSION

Here we show that loss of succinate-mediated signaling through SUCNR1 in myeloid cells impaired the induction of an anti-inflammatory program in macrophages and the response to type 2 cytokines, including those associated with diet-induced obesity[41, 42]

and long-term cold exposure[38, 40]. We showed that extracellular succinate acted in cooperation with IL-4 signaling through the activation of the PKA-CREB-KLF4 pathway and increased the IL-4 response in a cell-autonomous manner. Notably, *Sucnr1* deficiency altered the phenotype of ATMs in a manner dependent on the WAT localization, by promoting an inflammatory molecular signature in scWAT ATMs. Our results suggest a mechanism by which SUCNR1 signaling contributes to resolution of acute inflammation.

In response to metabolic and inflammatory challenge, succinate accumulates in pro-inflammatory macrophages[20, 43], which triggers an inflammatory phenotype through activation of HIF-1α[3]. In this scenario, succinate is exported to the extracellular milieu[23] where it signals through SUCNR1[2, 23]. Though intracellular succinate is considered a pro-inflammatory stimulus[2, 3, 23], our observations indicated that SUCNR1 was mostly expressed in pro-resolving or anti-inflammatory macrophages, as previously reported[44]. *LysM*-Cre *Sucnr1*$^{fl/fl}$ mice developed local tissue inflammation and deregulated glucose homeostasis at steady-state. Moreover, these mice showed higher susceptibility to develop diet-induced obesity compared with *Sucnr1*$^{fl/fl}$ mice. *Sucnr1*$^{-/-}$ mice have yielded contradictory results in terms of glucose homeostasis and susceptibility to develop obesity depending on HFD composition (45% vs 60% calories from fat)[10, 18]. Our results showed enhanced weight gain and impaired glucose tolerance in *LysM*-Cre *Sucnr1*$^{fl/fl}$ compared to control mice in response to 45% HFD. This contrasts with the phenotype observed in the global Sucnr1$^{-/-}$ mice fed with the same diet, in which there was a decrease of macrophage infiltration into adipose tissue and an improvement of glucose tolerance compared to control mice, despite similar increase in body weight[10]. These differences hightlight the importance of cell-specific studies assessed by conditional knockout mouse models to adequately evaluate the role of SUCNR1 in individual cell subsets.

Our data indicated that extracellular succinate promoted an anti-inflammatory program in macrophages. BMDMs, pMs and scWAT ATMs from the *LysM*-Cre *Sucnr1*$^{fl/fl}$ mice showed increased expression of pro-inflammatory markers (e.g. *Il1b, Il12b, Tnf* and *Nos2*) and did not upregulate expression of anti-inflammatory markers (e.g *Arg1*, *Mrc1*, *Fizz1*, *Il10*) in response to IL-4, as observed in *Sucnr1*$^{fl/fl}$ macrophages. This suggested that extracellular succinate triggered a pro-resolving phenotype in tissue-resident macrophages as ATMs, to counterbalance the inflammatory signals and recover metabolic homeostasis. Consistent with this notion, succinate has been proposed to act as

an “alarmin” for the innate immune system, more specifically in DCs[2, 22, 23]. Anti-inflammatory properties for signaling through SUCNR1 have been previously reported. For example, inflammatory macrophage-derived succinate signals through SUCNR1 in neural stem cells to induce production of prostaglandin E2, triggering the resolution of inflammation during chronic neuroinflammation in mice with experimental autoimmune encephalomyelitis[24]. Also, SUCNR1 signaling was reported as a potent activator of type 2 immunity and a surveillance mechanism for detection of certain helminthes as *Tritrichomonas* in the small intestine of C57BL/6 mice [25]. We propose a mechanism by which, similar to other signaling molecules such as IL-6[45, 46], succinate is generated as part of an inflammatory program and acts as a negative feedback signal through SUCNR1to promote an anti-inflammatory response in macrophages.

scWAT ATMs have a key role in metabolic homeostasis, and their remodeling is crucial to adequately respond to chronic positive energy balance[47, 48]. Our results indicated that in obese mice, loss of SUCNR1 in myeloid cells induced an inflammatory state in scWAT ATMs, but decreased the activation of inflammatory signaling pathways such as interferon and TNF response in vWAT ATMs. Comparative transcriptome profiling of ATMs from sc and vWAT from control mice revealed that vWAT ATMs were constitutively more inflamed than scWAT ATMs. This is consistent with the pro-inflammatory profile previously described in the visceral compared to the subcutaneous fat depots[37]. Activation of SUCNR1 was reported to have a positive effect on the release of the pro-inflammatory cytokine IL-1β in inflammatory macrophages. As such, during inflammation, succinate-SUCNR1 signaling may act as an anti-inflammatory mediator or boost inflammation[23] depending of inflammatory stauts of cells expressing SUCNR1. Our data showed that activation of SUCNR1 decreased the expression of inflammatory-related genes in the scWAT of healthy subjects, whereas scWAT from obese patients was insensitive to signaling through SUCNR1. Extracellular succinate increased the expression of inflammatory markers in the scWAT from obese patients, which is known to shift towards a pro-inflammatory phenotype[49]. Although obesity is characterized by high circulating amounts of succinate[11], ATMs from obese subjects had decreased expression of SUCNR1, along with other anti-inflammatory markers, such as PPARγ and MRC1. This “succinate-resistant state” in human obesity that might underlie, at least partially, the obesity-associated inflammation. The loss of this anti-inflammatory mechanism in obesity may contribute to the intrinsic inability of obese adipose tissue to

resolve uncontrolled inflammation and to restore tissue homeostasis and functionality[49, 50] . As succinate-SUCNR1 signaling is emerging as a versatile and context-specific regulator of physiology and disease, further research is needed to provide a complete picture on its local and systemic modes of action.

Acknowledgements

This study was supported by grants from the Spanish Ministry of Science, Innovation and Universities (PI14/00228 and PI17/01503 to JV, SAF2015-65019-R to SF-V, SAF2014-56819-R and SAF2015-71878-REDT to AC, BFU2016-78951-R to GM-M, PI15/00143 to CS and PI15/01562 to AM, BFU2015-70454-REDT and BFU2017-90578-REDT to SF-V and GM-M) co-financed by the European Regional Development Fund (ERDF). The Spanish Biomedical Research Center in Diabetes and Associated Metabolic Disorders (CIBERDEM) (CB07708/0012) is an initiative of the Instituto de Salud Carlos III. NK is recipient of a predoctoral fellowship from MINECO, Spain (FPI, BES-2016-077745). CS acknowledges support from the ‘‘Ramón y Cajal’ program from MINECO (RYC2013-13186) and SF-V the Miguel Servet tenure-track program (CP10/00438 and CPII16/00008) from the Fondo de Investigación Sanitaria, co-financed by the ERDF. We want to particularly acknowledge the patients and the BioBank IISPV (PT17/0015/0029) integrated in the Spanish National Biobanks Network for its collaboration. We also thank K. McCreath and A. Cervera for kindly providing the C57BL/6 *Sucnr1*$^{fl/fl}$ mice and for their helpful comments on the manuscript. Finally, we thank IRB Barcelona Functional Genomics Core Facility for Microarray processing and IRB Barcelona Biostatistics and Bioinformatics facility.

Author Contributions

JV and SF-V conceived, designed and supervised the research project. NK, VC-M and EC participated in the conception and design of the study, sample collection, experiment planning and conduction. CS analyzed human metabolic data. ME performed flow cytometry data acquisition and analysis of data. MIH-A carried out transcriptome analysis. JVdR analysed ChIP-seq genomic data. RF and RJ participated in the human sample recruitment. DH provided technical assistance and analysis of data of the metabolic phenotype study in mice. CN-R, EM-M and MMR performed cell culture and technical animal procedures assistance. AZ, AC, AM, GM-G and CS provided scientific discussion and revised the manuscript. SF-V and JV are the guarantors of this work.

Competent interests

The authors declare that there is no conflict of interest regarding the publication of this article

REFERENCES

1. Chouchani, E.T. *et al.* Ischaemic accumulation of succinate controls reperfusion injury through mitochondrial ROS. *Nature* **515**, 431-435 (2014).

2. Rubic, T. *et al.* Triggering the succinate receptor GPR91 on dendritic cells enhances immunity. *Nat Immunol* **9**, 1261-1269 (2008).

3. Tannahill, G.M. *et al.* Succinate is an inflammatory signal that induces IL-1beta through HIF-1alpha. *Nature* **496**, 238-242 (2013).

4. Toma, I. *et al.* Succinate receptor GPR91 provides a direct link between high glucose levels and renin release in murine and rabbit kidney. *J Clin Invest* **118**, 2526-2534 (2008).

5. Murphy, M.P. & O'Neill, L.A.J. Krebs Cycle Reimagined: The Emerging Roles of Succinate and Itaconate as Signal Transducers. *Cell* **174**, 780-784 (2018).

6. Peti-Peterdi, J., Gevorgyan, H., Lam, L. & Riquier-Brison, A. Metabolic control of renin secretion. *Pflugers Arch* **465**, 53-58 (2013).

7. Hochachka, P.W. & Dressendorfer, R.H. Succinate accumulation in man during exercise. *Eur J Appl Physiol Occup Physiol* **35**, 235-242 (1976).

8. Sadagopan, N. *et al.* Circulating succinate is elevated in rodent models of hypertension and metabolic disease. *Am J Hypertens* **20**, 1209-1215 (2007).

9. Aguiar, C.J. *et al.* Succinate causes pathological cardiomyocyte hypertrophy through GPR91 activation. *Cell Commun Signal* **12**, 78 (2014).

10. van Diepen, J.A. *et al.* SUCNR1-mediated chemotaxis of macrophages aggravates obesity-induced inflammation and diabetes. *Diabetologia* **60**, 1304-1313 (2017).

11. Serena, C. *et al.* Elevated circulating levels of succinate in human obesity are linked to specific gut microbiota. *ISME J* (2018).

12. He, W. *et al.* Citric acid cycle intermediates as ligands for orphan G-protein-coupled receptors. *Nature* **429**, 188-193 (2004).

13. Gilissen, J., Jouret, F., Pirotte, B. & Hanson, J. Insight into SUCNR1 (GPR91) structure and function. *Pharmacol Ther* **159**, 56-65 (2016).

14. de Castro Fonseca, M., Aguiar, C.J., da Rocha Franco, J.A., Gingold, R.N. & Leite, M.F. GPR91: expanding the frontiers of Krebs cycle intermediates. *Cell Commun Signal* **14**, 3 (2016).

15. Sapieha, P. *et al.* The succinate receptor GPR91 in neurons has a major role in retinal angiogenesis. *Nat Med* **14**, 1067-1076 (2008).

16. Vargas, S.L., Toma, I., Kang, J.J., Meer, E.J. & Peti-Peterdi, J. Activation of the succinate receptor GPR91 in macula densa cells causes renin release. *J Am Soc Nephrol* **20**, 1002-1011 (2009).

17. Li, Y.H., Woo, S.H., Choi, D.H. & Cho, E.H. Succinate causes alpha-SMA production through GPR91 activation in hepatic stellate cells. *Biochem Biophys Res Commun* **463**, 853-858 (2015).

18. McCreath, K.J. *et al.* Targeted disruption of the SUCNR1 metabolic receptor leads to dichotomous effects on obesity. *Diabetes* **64**, 1154-1167 (2015).

19. Hakak, Y. *et al.* The role of the GPR91 ligand succinate in hematopoiesis. *J Leukoc Biol* **85**, 837-843 (2009).

20. Ryan, D.G. & O'Neill, L.A.J. Krebs cycle rewired for macrophage and dendritic cell effector functions. *FEBS Lett* **591**, 2992-3006 (2017).

21. Saraiva, A.L. *et al.* Succinate receptor deficiency attenuates arthritis by reducing dendritic cell traffic and expansion of Th17 cells in the lymph nodes. *FASEB J*, fj201800285 (2018).

22. Rubic-Schneider, T. *et al.* GPR91 deficiency exacerbates allergic contact dermatitis while reducing arthritic disease in mice. *Allergy* **72**, 444-452 (2017).

23. Littlewood-Evans, A. *et al.* GPR91 senses extracellular succinate released from inflammatory macrophages and exacerbates rheumatoid arthritis. *J Exp Med* **213**, 1655-1662 (2016).

24. Peruzzotti-Jametti, L. *et al.* Macrophage-Derived Extracellular Succinate Licenses Neural Stem Cells to Suppress Chronic Neuroinflammation. *Cell Stem Cell* (2018).

25. Lei, W. *et al.* Activation of intestinal tuft cell-expressed Sucnr1 triggers type 2 immunity in the mouse small intestine. *Proc Natl Acad Sci U S A* **115**, 5552-5557 (2018).

26. Shan, B. *et al.* The metabolic ER stress sensor IRE1alpha suppresses alternative activation of macrophages and impairs energy expenditure in obesity. *Nat Immunol* **18**, 519-529 (2017).

27. Manieri, E. & Sabio, G. Stress kinases in the modulation of metabolism and energy balance. *J Mol Endocrinol* **55**, R11-22 (2015).

28. Arch, J.R., Hislop, D., Wang, S.J. & Speakman, J.R. Some mathematical and technical issues in the measurement and interpretation of open-circuit indirect calorimetry in small animals. *Int J Obes (Lond)* **30**, 1322-1331 (2006).

29. Virtue, S. & Vidal-Puig, A. Assessment of brown adipose tissue function. *Front Physiol* **4**, 128 (2013).

30. Mills, E.L. *et al.* Succinate Dehydrogenase Supports Metabolic Repurposing of Mitochondria to Drive Inflammatory Macrophages. *Cell* **167**, 457-470 e413 (2016).

31. Hamilton, T.A., Zhao, C., Pavicic, P.G., Jr. & Datta, S. Myeloid colony-stimulating factors as regulators of macrophage polarization. *Front Immunol* **5**, 554 (2014).

32. Jaguin, M., Houlbert, N., Fardel, O. & Lecureur, V. Polarization profiles of human M-CSF-generated macrophages and comparison of M1-markers in classically activated macrophages from GM-CSF and M-CSF origin. *Cell Immunol* **281**, 51-61 (2013).

33. Liao, X. *et al.* Kruppel-like factor 4 regulates macrophage polarization. *J Clin Invest* **121**, 2736-2749 (2011).

34. Luan, B. *et al.* CREB pathway links PGE2 signaling with macrophage polarization. *Proc Natl Acad Sci U S A* **112**, 15642-15647 (2015).

35. Avni, D., Ernst, O., Philosoph, A. & Zor, T. Role of CREB in modulation of TNFalpha and IL-10 expression in LPS-stimulated RAW264.7 macrophages. *Mol Immunol* **47**, 1396-1403 (2010).

36. Boutens, L. & Stienstra, R. Adipose tissue macrophages: going off track during obesity. *Diabetologia* **59**, 879-894 (2016).

37. Kwok, K.H., Lam, K.S. & Xu, A. Heterogeneity of white adipose tissue: molecular basis and clinical implications. *Exp Mol Med* **48**, e215 (2016).

38. Qiu, Y. *et al.* Eosinophils and type 2 cytokine signaling in macrophages orchestrate development of functional beige fat. *Cell* **157**, 1292-1308 (2014).

39. Fabbiano, S. *et al.* Caloric Restriction Leads to Browning of White Adipose Tissue through Type 2 Immune Signaling. *Cell Metab* **24**, 434-446 (2016).

40. Hui, X. *et al.* Adiponectin Enhances Cold-Induced Browning of Subcutaneous Adipose Tissue via Promoting M2 Macrophage Proliferation. *Cell Metab* **22**, 279-290 (2015).

41. Fujisaka, S. *et al.* Regulatory mechanisms for adipose tissue M1 and M2 macrophages in diet-induced obese mice. *Diabetes* **58**, 2574-2582 (2009).

42. Odegaard, J.I. *et al.* Alternative M2 activation of Kupffer cells by PPARdelta ameliorates obesity-induced insulin resistance. *Cell Metab* **7**, 496-507 (2008).

43. Mills, E.L., Kelly, B. & O'Neill, L.A.J. Mitochondria are the powerhouses of immunity. *Nat Immunol* **18**, 488-498 (2017).

44. Trauelsen, M. *et al.* Receptor structure-based discovery of non-metabolite agonists for the succinate receptor GPR91. *Mol Metab* **6**, 1585-1596 (2017).

45. Mauer, J. *et al.* Signaling by IL-6 promotes alternative activation of macrophages to limit endotoxemia and obesity-associated resistance to insulin. *Nat Immunol* **15**, 423-430 (2014).

46. Reilly, S.M. & Saltiel, A.R. Countering inflammatory signals in obesity. *Nat Immunol* **15**, 410-411 (2014).

47. Pellegrinelli, V., Carobbio, S. & Vidal-Puig, A. Adipose tissue plasticity: how fat depots respond differently to pathophysiological cues. *Diabetologia* **59**, 1075-1088 (2016).

48. Carobbio, S., Pellegrinelli, V. & Vidal-Puig, A. Adipose Tissue Function and Expandability as Determinants of Lipotoxicity and the Metabolic Syndrome. *Adv Exp Med Biol* **960**, 161-196 (2017).

49. Lumeng, C.N., DelProposto, J.B., Westcott, D.J. & Saltiel, A.R. Phenotypic switching of adipose tissue macrophages with obesity is generated by spatiotemporal differences in macrophage subtypes. *Diabetes* **57**, 3239-3246 (2008).

50. Wellen, K.E. & Hotamisligil, G.S. Obesity-induced inflammatory changes in adipose tissue. *J Clin Invest* **112**, 1785-1788 (2003).

FIGURE LEGENDS

Figure 1. *LysM*-Cre *Sucnr1*$^{fl/fl}$ mice fed a NCD show tissue inflammation and glucose intolerance. (**a**) qPCR analysis of *Sucnr1* mRNA in BMDMs, pMs, scWAT ATMs and vWAT ATMs in *LysM*-Cre *Sucnr1*$^{fl/fl}$ mice and age-matched *Sucnr1*$^{fl/fl}$ littermates (BMDMs and pMs n=5 or 4; scWAT n=4; vWAT n=3 or 4, for *Sucnr1*$^{fl/fl}$ and *LysM*-Cre *Sucnr1*$^{fl/fl}$ respectively; biologically independent samples). Results are transformed as $\log_2$(value+1) relative to BMDMs from *Sucnr1*$^{fl/fl}$ mice, set as 1. (**b**) Body weight progression. (**c**) Changes in body weight and fasting serum glucose as in (**a**) from two independent experiments (n=10 mice). Serum insulin levels as in (**a**) (n=5 for *Sucnr1*$^{fl/fl}$ and n=4 for *LysM-Sucnr1*$^{-/-}$ mice). (**d**) GTT, (**e**) ITT and their respective area under the curve (AUC) as in (**a**) (n=4 mice). (**f**) qPCR analysis of pro-inflammatory (n=6 for *Sucnr1*$^{fl/fl}$ and n=5 for *LysM-Sucnr1*$^{-/-}$ mice) and (**g**) anti-inflammatory genes (n=7 mice) as in (**a**) from two independent experiments. (**h**) Abundance of CD11b^{+}F4/80^{+} cells assessed by flow cytometry in scWAT and vWAT SVF (n=3 biologically independent samples). (**i**) Immunoblot analysis of phosphorylated (p-)JNK1/2 protein. β-actin used as loading control. Representative image and densitometry analysis (AU, arbitrary units) (n=5 per *Sucnr1*$^{fl/fl}$ and n=6 per *LysM*-Cre *Sucnr1*$^{fl/fl}$ biologically independent samples). Uncropped blots are provided in source data. All data are shown as mean ± SEM; *P < 0.05; **P < 0.01; ***P < 0.001; ns: non-significant (two-tailed unpaired t-test in bar graphs and two-way ANOVA in body weight, GTT and ITT curves).

Figure 2. *LysM*-Cre *Sucnr1*$^{fl/fl}$ mice on HFD are prone to develop obesity, glucose intolerance and insulin sensitivity. (**a**) Body weight progression in *LysM*-Cre *Sucnr1*$^{fl/fl}$ mice and age-matched *Sucnr1*$^{fl/fl}$ littermates fed a HFD for 18 weeks (n=9 mice), (**b**) Fasting plasma succinate in *LysM*-Cre *Sucnr1*$^{fl/fl}$ and *Sucnr1*$^{fl/fl}$ mice fed a HFD or NCD (n=4 for *Sucnr1*$^{fl/fl}$ and n=5 for *LysM*-Cre *Sucnr1*$^{fl/fl}$ on NCD; n=4 mice on HFD) (left) and qPCR analysis of *Sucnr1* mRNA in scWAT (n=4 for *Sucnr1*$^{fl/fl}$ and n=3 for *LysM*-Cre *Sucnr1*$^{fl/fl}$ on NCD; n=4 mice on HFD) and scWAT ATMs as in (**a**) (right) (n=4 biologically independent samples). (**c**) Immunohistochemical staining of F4/80^{+} cells in scWAT and vWAT as in (**a**). Representative images from two independent experiments (n=4 mice). Scale bars, 1 mm. (**d**) EE (left) and RER (right) during light and dark hours, as in (**a**) (n=5 mice). (**e**) Fasting serum glucose (n=9 mice) and insulin levels (n=5 mice) as in (**a**). (**f**) GTT (n=8 *Sucnr1*$^{fl/fl}$; n=6 *LysM*-Cre *Sucnr1*$^{fl/fl}$) and (**g**) ITT and their

respective AUC (n=8 *Sucnr1*$^{fl/fl}$; n=5 *LysM*-Cre *Sucnr1*$^{fl/fl}$) (**f-g**) as in (**a**). (**h-i**) qPCR analysis of pro-inflammatory (n=4 mice) (**h**) and anti-inflammatory (n=6 mice) (**i**) genes in scWAT, vWAT and liver as in (**a**) from two independent experiments. Results are expressed as mean ± SEM; *P < 0.05; **P < 0.01; ***P < 0.001; ns: non-significant (two-tailed unpaired t-test in bar graphs and two-way ANOVA in body weight, GTT and ITT curves).

Figure 3. **Signaling by succinate *via* SUCNR1 promotes an anti-inflammatory macrophage program in a cell-autonomous manner.** (**a**) Succinate secretion in 24 hr conditioned medium (CM) (left) and *Sucnr1* mRNA expression (right) of pMs from *Sucnr1*$^{fl/fl}$ mice, without stimulation or stimulated with LPS or IL-4 for 6 hr (n=4). (**b**) Succinate secretion in 24 hr CM (left) and *SUCNR1* mRNA expression (right) in human PBMCs (hPBMCs) non-differentiated (control) or differentiated with GM-CSF or M-CSF for 7 d (n=3). (**c**) *SUCNR1* mRNA expression hPBMCs differentiated with M-CSF, and then unstimulated or stimulated for 24 hr with LPS or IL-4 (n=3). (**d**) qPCR mRNA analysis of selected genes in pM from *Sucnr1*$^{fl/fl}$ and *LysM*-Cre *Sucnr1*$^{fl/fl}$ mice (n=3); (**e**) qPCR analysis in pM following IL-4 stimulation for 6 hr (n=3). Results are expressed relative to a basal state represented as 1. (**f**) qPCR mRNA analysis in *Sucnr1*$^{fl/fl}$ and *LysM*-Cre *Sucnr1*$^{fl/fl}$ BMDMs stimulated with M-CSF for 7 d (n=3), relative to their respective basal expression as 1; (**g**) qPCR mRNA analysis in BMDM$^{M\text{-}CSF}$ stimulated with succinate (200 μM) overnight (n=4). (**a-f**) n represents biologically independent samples. Data are shown as mean ± SEM; *P < 0.05; **P < 0.01; ***P < 0.001 (two-tailed unpaired t-test).

Figure 4. SUCNR1 signaling in macrophages. (**a**) *SUCNR1* mRNA in THP1 cells transfected with siRNAs (control, STAT6 and KLF4) and stimulated with IL-4 for 6 hr (Ctrl: n=4; STAT6 and KLF4 n=3). qPCR analysis of (**b**) Expression of *Sucnr1* in *Sucnr1*$^{fl/fl}$ BMDMs (n=6) and *Stat6*$^{-/-}$ BMDMs (n=3) and (**c**) *Sucnr1*$^{fl/fl}$ BMDMs transfected with siRNAs for STAT6 (n=4), KLF4 (n=4) or control vector (Ctrl, n=8) after stimulation with IL-4. (**d-f**) Immunoblot analysis of selected proteins in *Sucnr1*$^{fl/fl}$ BMDMs transfected with control and KLF4 siRNAs(**d**), *Sucnr1*$^{fl/fl}$ BMDMs pre-treated with H-89 for 30 min **(e)** and *LysM*-Cre *Sucnr1*$^{fl/fl}$ BMDMs stimulated with succinate **(f)**. (**g**) qPCR analysis of selected genes in *Sucnr1*$^{fl/fl}$ BMDMs pretreated with H-89 or transfected with siRNAs-KLF4 after succinate stimulation for 6 hr (n=3/group, except

n=4 for *Il10* mRNA in KLF4 with succinate). (**h,i**) Immunoblot analysis of *LysM*-Cre *Sucnr1*$^{fl/fl}$ and *Sucnr1*$^{fl/fl}$ BMDMs pre-incubated with succinate for 2 hr (**h**) and *Sucnr1*$^{fl/fl}$ BMDMs treated with H-89 and pre-incubated with succinate (**i**); (**j**) Expression of *Il10* and *Arg1* in *Sucnr1*$^{fl/fl}$ BMDMs pre-treated with succinate and H-89 (n=3 and n=4 for *Il10* mRNA in control without H-89). Results are represented relative to respective basal expression as 1 (without IL-4 in **a-c**, **j**; without succinate stimulation in **g**). (**d-e,f,h-i**) Representative image and densitometry analysis (AU). (**a-j)** n represents biologically independent samples. **(a-c, g, j)** Values are expressed as mean ± SEM; *P < 0.05; **P < 0.01; ***P < 0.001; ns: non-significant (two-tailed unpaired t-test). For immunoblots, GAPDH was used as the loading control. Uncropped blots are provided in source data. Values are expressed as mean ± SEM; (**d, e, h; #** *P*<0.05 versus time 0 (two-tailed paired t-test), * *P*<0.05 versus ctrl).

Figure 5. ***LysM*-Cre *Sucnr1*$^{fl/fl}$ deficient ATMs show an altered transcriptome signature.** (**a**) Volcano plots for microarray gene expression of scWAT and vWAT ATMs from *LysM*-Cre *Sucnr1*$^{fl/fl}$ and *Sucnr1*$^{fl/fl}$ mice. Linear models with empirical Bayes statistic (Limma) where used for differential expression. Genes in red have BH adjusted p-value <0.05. (**b**) Heatmap with GSEA normalized enrichment scores (and significance) for ATMs as in (**a**) on Hallmark gene sets. P-values were calculated by gene set permutations. FDR +/ */ **/*** for 0.25/ 0.10/ 0.05/ 0.01, respectively. (**c**) Barplots showing enrichment scores ($-\log_{10}$ of FDR p-values (signed)) of Hallmarks (GSEA) distinguishing between downregulated (shown in negative) and upregulated (shown in positive) pathways (filtered by genesets with FDR < 0.25) for ATMs as in (**a**). (**a-c**) n=4 biologically independent samples. (**d-f**) qPCR analysis of selected genes in (**d**) ATMs as in (**a**); (**g**) $Cd11b^+/CD11c^+/CD206^-$ and (**h**) $Cd11b^+/CD11c^-/CD206^+$ cell populations from ATMs as in (**a**). (**d**, n=4 or 3; **e**, n=7 or 5 and **f**, n=5 for *Sucnr1*$^{fl/fl}$ and *LysM*-Cre *Sucnr1*$^{fl/fl}$ respectively, biologically independent samples). Data are expressed as mean ± SEM; *P < 0.05; **P < 0.01; ***P < 0.001 (two-tailed unpaired t-test).

Figure 6. Sucnr1-deficient subcutaneous adipose tissue-resident macrophages are unresponsive to IL-4 and succinate. (**a**) qPCR analysis of selected genes in scWAT ATMs from *Sucnr1*$^{fl/fl}$ and *LysM*-Cre *Sucnr1*$^{fl/fl}$ mice fed a NCD or HFD stimulated with IL-4 for 6 hr (n=3 for NCD and n=4 for HFD, except n=3 in *Il1rn* mRNA in *Sucnr1*$^{fl/fl}$). (**b**) qPCR analysis of selected genes as in (**a**) stimulated with succinate for 6 hr (n=4,

except n=3 for *Sucnr1* mRNA). (**c**) qPCR analysis of selected genes as in (**a**) stimulated with LPS for 6 hr (n=4, except n=3 for *Il6* mRNA). (**d**) qPCR analysis of gene expression of *Il10* and *Sucnr1* in scWAT ATMs on a NCD, pretreated or not with H-89 (30 min) before stimulation with succinate for 6 hr (n=4, except n=3 for *Sucnr1* mRNA in H-89). (**e**) qPCR analysis of gene expression of *Il10* and *Sucnr1* as in (**d**), transfected with siRNA against KLF4 or control (Ctrl) before stimulation with succinate for 6 hr (n=4, except n=3 for *Sucnr1* mRNA in KLF4). Results are presented relative to their respective basal expression as 1 (without IL-4 in (**a**), without succinate in (**b,d,e)** and without LPS in (**c**). (**a-e**) n represents biologically independent samples. Values are expressed as mean ± SEM, in (**b-e**) data are $\log_2$ (value+1) transformed; *P < 0.05; **P < 0.01; ***P < 0.001 (two-tailed unpaired t-test).

Figure 7. ***LysM*-Cre *Sucnr1*$^{fl/fl}$ mice are refractory to prolonged cold-induced browning in scWAT.** (**a**) qPCR analysis of *Ucp1* and typical markers of beige activation in scWAT from male *Sucnr1*$^{fl/fl}$ and *LysM*-Cre *Sucnr1*$^{fl/fl}$ mice housed at 8ºC or 22ºC for 6 days (n=3 mice at 22ºC; n=4 for *Sucnr1*$^{fl/fl}$ and n=5 for *LysM*-Cre *Sucnr1*$^{fl/fl}$ at 8ºC). Results are transformed as $\log_2$(value+1) normalized to gene expression of *Sucnr1*$^{fl/fl}$ mice at 22ºC. (**b**) Representative images of immunohistochemical staining of UCP1 in scWAT as in **(a)** housed at 8ºC, from two independent experiments (n=4 mice). Scale bars, 200μm. (**c**) Representative images of immunoblot analysis of UCP1 in scWAT (left) as in (**a**) and quantification performed as the ratio of UCP1/FAA presented in AU (right) (n=2 mice). (**d**) qPCR analysis of *Ucp1* in BAT as in **(a)** (n=3 per genotype at 22ºC and n=4 per genotype at 8ºC). (**e**) Representative images of immunohistochemical staining of UCP1 in BAT from two independent experiments (n=4 mice). Scale bars, 200μm (left) and immunoblot analysis of UCP1 protein in BAT (right) and quantification performed as the ratio of UCP1/FAA presented in AU (n=2 mice). Representative results from two independent experiments with similar results. Uncropped blots are provided in source data. (**f**) Energy Expenditure (EE) and oxygen consumption (VO_2) of *Sucnr1*$^{fl/fl}$ and *LysM*-Cre *Sucnr1*$^{fl/fl}$ mice acutely subjected to 8ºC from thermoneutrality (30ºC). Data are shown as mean ± SEM; *P < 0.05; **P < 0.01; ***P < 0.001 (two-tailed unpaired t-test).

Figure 8. Obese human adipose tissue is insensitive to the anti-inflammatory effects of succinate. (**a**) qPCR analysis of expression of *SUCNR1* in scWAT and vWAT from

human lean (n=15 for sc and n=13 for vWAT) and obese (n=36 for sc and n=27 for vWAT) patients. (**b**) Correlation between *SUCNR1* gene expression in scWAT with glucose (n=46), hip circumference (n=28) and diastolic blood pressure (DBP) (n=19) from human patients. (**c,d**) qPCR analysis of expression of *SUCNR1* in subcutenous adipocytes (scAD) or visceral adipocytes (vAD) (**c**) and scWAT ATMs from lean and obese patients (**d**) (n=4, n=3 and n=3). (**e**) qPCR analysis of selected genes in human scWAT ATMs (n=3). (**f,g**) qPCR analysis of pro-inflammatory genes in human scWAT explants, unstimulated or stimulated with succinate for 24 hr, from lean (**f**) and obese (**g**) patients (n=2 and n=3 for expression of *ILB* in scWAT derived from a pool of 3 patients per phenotype). **(a-g)** n represents biologically independent samples. Results are expressed as mean ± SEM; *P < 0.05; **P < 0.01; ***P < 0.001 (two-tailed unpaired t-test). For (**b**) Spearman's (in glucose and HIP graph) or Pearson's (in DBP graph) correlation analysis was used.

METHODS

Also see Life Sciences Reporting Summary for details

Human cohort

All participants gave their informed consent and the study was reviewed and approved by the Ethics and Research Committee of Institut d´Investigació Sanitària Pere Virgili (IISPV CEIm, Tarragona, Spain), in accordance with Good Clinical Practice Guidelines approved by the Health Department of Generalitat de Catalunya, which met all requirements of the Declaration of Helisnki. Donors were classified as lean or obese based on body mass index (BMI) following World Health Organization criteria. Plasma, scWAT and vWAT were obtained from age- and gender-matched human donors undergoing non-acute surgical interventions, such as hernia or cholecystectomy, in a scheduled routine surgery: lean n=15 (BMI 22.87±1.51); obese n=36 (BMI 31.44±4.55). Anthropometric and biochemical variables from the cohort are represented in **Supplementary Table 3**.

Mice

Myeloid cell-specific *Sucnr1* KO mice (*LysM*-Cre *Sucnr1*$^{fl/fl}$) were generated by breeding *LysM*-Cre mice (kindly provided by G. Sabio; CNIC, Spain) with *Sucnr1*$^{fl/fl}$ mice. Cre-

negative *Sucnr1*$^{fl/fl}$ littermates were used as controls. Mice were genotyped by PCR; genotyping of *Sucnr1*$^{fl/fl}$ mice resulted in a 450-base pair product for the loxP-targeted allele and a 300-base pair product for the wild-type allele. All genotypes were generated on a pure C57BL/6 background. Total *Stat6*$^{-/-}$ mice in a C57BL/6 background were purchased from The Jackson Laboratory (Ban Harbor, ME). Mice were housed at the Faculty of Medicine and Health Science animal facility, Rovira i Virgili University (URV). Male mice were grouped (5 per cage) under controlled conditions of 12 hr light/dark cycles at 22°C and *ad libitum* access to NCD (3.1% fat; SAFE diets, A04) or HFD (45% fat; Research diets, D12451), beginning at 7 weeks of age. All animal studies were supervised and approved by the Universitat Rovira i Virgili Animal Welfare and Ethics Committee. All animal procedures conformed to EU Directive 86/609/EEC and recommendation 2007/526/EC regarding the protection of animals used for experimental and other scientific purposes, enacted under Spanish law 1201/2005.

Indirect calorimetry and activity measurements

Animals were placed in a comprehensive laboratory animal monitoring system (PhenoMaster, TSE Systems, Germany) for analysis of metabolic phenotypes of male *Sucnr1*$^{fl/fl}$ and *LysM-Sucnr1*$^{fl/fl}$ mice (at 22°C), and at 22°C, 30°C and 8°C for the cold exposure study. Airflow rate was 380 ml/min; O_2 and CO_2 concentrations in room air and air leaving each cage were measured every 15 min. Energy expenditure (EE, kcal/h/mouse or kcal/h/kg) was calculated from the amount of O_2 consumed (VO_2, ml/h/mouse or ml/h/kg, respectively) and the amount of CO_2 produced (VCO_2) using the equation: EE (J) = $15.818VO_2 + 5.176VCO_2$. The respiratory exchange rate (RER) was calculated from the ratio VCO_2/VO_2. Activity, food and drink intake of each animal was calculated as described[51]. Data for EE were analyzed using analysis of covariance (ANCOVA) with body weight as a covariate.

Glucose and insulin tolerance test

After 16 hr of fasting, mice were subjected to a glucose tolerance test, receiving an intraperitoneal injection of glucose solution (1.5 g glucose/kg body weight). Blood was collected from the tail and glucose was measured using a handheld glucometer (Accu-Chek glucose reader; Roche, Mannheim, Germany). To measure insulin levels in response to glucose, blood was collected from tail punctures at 0, 15 and 30 min post-injection and insulin was measured using a commercial Mouse Insulin Ultra-Sensitive

ELISA (BioVendor, Brno, Czech Republic). For the intraperitoneal insulin tolerance test, mice were fasted for 3 hr and injected with insulin (0.75 U/kg).

Isolation of mature adipocytes, stromal vascular fraction and adipose tissue macrophages

ATMs were isolated from the SVF of human adipose tissue biopsies as described[52, 53]. Briefly, scWAT and vWAT was washed extensively with PBS to remove debris and treated with 0.1% collagenase in PBS and 1% BSA for 1 hr at 37°C with gentle agitation. Digested samples were centrifuged at 300 × *g* at 4°C for 5 min to separate adipocytes from the SVF. Adipocytes were directly used for RNA isolation and the cell pellet containing the SVF was resuspended in red-blood-cell lysis buffer (10 mM $KHCO_3$, 150 mM NH_4Cl, 0.1 mM EDTA) for 2 min, then washed with PBS and passed through a 40-μm filter (Fisher Scientific). To isolate ultrapure ATMs, the SVF was incubated with F4/80 MicroBeads (130-110-443, MiltenyiBiotec S.L. Madrid, Spain) for 30 min and positive selection was performed with an autoMACS separator (MiltenyiBiotec). Each biologically independent sample was obtained from a pool of 6-7 mice (*Sucnr1*$^{fl/fl}$ or *LysM*-Cre *Sucnr1*$^{fl/fl}$), or 2-3 human individuals samples (lean or obese).

Isolation and culture of adipose tissue explants

Human adipose tissue samples were obtained as described above. Mouse scWAT and vWAT was freshly isolated and 0.2 g of tissue was placed in 1 ml DMEM/F12 and 10% fetal bovine serum (FBS). Samples were incubated for 24 hr at 37°C and 5% CO_2 without or with succinate at 200 μM. Each biologically independent sample was obtained from a pool of 2-3 mice (*Sucnr1*$^{fl/fl}$ or *LysM*-Cre *Sucnr1*$^{fl/fl}$), or human individuals samples (lean or obese).

Flow cytometry

The SVF from scWAT and vWAT was isolated as described above. To isolate myeloid lineage cells, SVF was incubated with CD11b MicroBeads (130-049-601, MiltenyiBiotec) for 30 min, and positive selection was performed with an autoMACS separator. Magnetically isolated $CD11b^+$ cells were washed and incubated with the desired combination of fluorochrome-conjugated monoclonal antibodies, including FITC-anti-F4/80 (clone BM8), APC-anti-CD11c (clone N418), PE-anti-CD206 (clone

MR6F3) and PE-Cy7-anti-Ly-6G (clone RB6-8C5) (all from eBiosciences, San Diego, CA) for 20 min. Data were acquired on a FACS Aria III (BD Biosciences) and analysis was performed using FACSDivaTM software (BD Biosciences).

Isolation and culture of human monocytes

Human PBMCs were isolated using Ficoll-Hypaque gradients (Amersham Bioscience, Barcelona. Spain). Monocytes were purified from PBMCs by magnetic cell sorting using CD14-microbeads (MiltenyiBiotech) as described[54]. Human PBMC-derived Mϕ were obtained by culturing $CD14^+$ cells in RPMI medium supplemented with human recombinant M-CSF or GM-CSF (30 ng/ml; PeproTech, Rocky Hill, NJ) for 7 days at 37ºC, refreshed every 2 days. Each biologically independent sample was obtained from a pool of 2-3 human individuals samples.

Isolation of peritoneal macrophages

Mice were euthanized by CO_2 inhalation. Resident peritoneal cells were harvested by lavage with 5 ml ice-cold PBS as described[55]. At 72 hr, cells mainly comprised peritoneal macrophages[56]. Macrophages were purified by adherence to tissue culture plates using an established procedure that gives >90% purity[56]. Non-adherent cells were removed by washing twice with PBS. Each biologically independent sample was obtained from a pool of 6-7 mice (*Sucnr1*$^{fl/fl}$ or *LysM*-Cre *Sucnr1*$^{fl/fl}$).

Isolation of bone marrow-derived macrophages

BMDMs from 8–11-week-old mice were obtained as described[57]. Briefly, mice were euthanized by CO_2 and the femurs and tibiae were collected and ground gently with a sterile mortar in 5 ml ice-cold PBS. Supernatants were collected in ice-cold PBS and filtered through a 70-μm nylon cell strainer to remove solid fragments. The filtrate was centrifuged at 450 × *g* for 10 min at 4°C, and pellets were dissociated in 10 ml red-blood-cell lysis buffer for 30 sec. After centrifugation, the pellet was dissociated in 20 ml of RPMI, 10% FBS and 1% antibiotic/antimycotic solution at 37°C, and cultured in 100-mm Petri-dishes for 4 hr at 37°C to remove resident bone marrow macrophages by adhesion. Collected supernatants were filtered and centrifuged as described above. Pellets were dissociated in RPMI supplemented with murine recombinant M-CSF or GM-CSF (30 ng/ml) and harvested after 7 days at 37°C with 5% CO_2. Media and stimuli were

refreshed every 2 days. Cells were placed in RPMI medium without stimulus for 24 hr prior to treatments. Differentiation was confirmed by F4/80 expression using flow cytometry (data not shown). Each biologically independent sample was obtained from a pool of 6-7 mice (*Sucnr1*$^{fl/fl}$ or *LysM*-Cre *Sucnr1*$^{fl/fl}$).

THP1 cell culture

The human monocyte THP-1 cell line was obtained from the ATCC (Rockville, MD). Cells were cultured as described[53]. Briefly, cells were cultured in RMPI-1640 medium supplemented with 10% FBS and 1% antibiotic/antimycotic solution in a humidified cell culture incubator at 37ºC with 5% CO_2.

Macrophage differentiation and stimulation

To assess gene expression of pro- and anti-inflammatory markers, human PBMCs and murine BMDMs treated with M-CSF were stimulated with *E. coli*-derived lipopolysaccharide (serotype 0111:B4, #L4391, Sigma-Aldrich, St Louis, MO) (250 ng/ml) or human or murine recombinant IL-4 (PeproTech) (30 ng/ml), respectively, for 24 hr. For succinate (200 μM), lipopolysaccharide (250 ng/ml) or IL-4 (30 ng/ml) treatment of ATMs, peritoneal macrophages and THP1, cells were stimulated for 6 hr. For cell signaling studies, BMDMs$^{M\text{-}CSF}$ were untreated or pre-incubated with a PKA inhibitor (H-89; #037M4702V, Sigma) (50 μM) for 30 min and/or succinate (200 μM) for 2 hr and subsequently exposed to IL-4 for the indicated time points. For succinate signaling, cells were untreated or pre-treated with H-89 and then stimulated with succinate for the indicated time points.

STAT6 and KLF4 silencing

THP1 cells were transfected with human STAT6 siRNA (#6778), KLF4 siRNA (#9314) or a control (non-targeting pool, #16600) using Dharmafect transfection reagent diluted in Opti-MEM I reduced serum medium (Invitrogen, Carlsbad, CA), added to the cultured cells for 48–72 hrs. BMDMs and ATMs were transfected with mouse STAT6 siRNA (#20852), KLF4 siRNA (#16600) or a control (Accell non-targeting pool, #D-001910-1050) using Accell siRNA delivery media (#B-005000-100), added to the cultured cells for 48–72 hrs. siRNAs were purchased from Dharmacon (Lafayette, CO, USA).

Succinate determination

Succinate levels were measured in plasma from humans and mice and also from conditioned medium from human PBMCs and murine BMDMs after 24 hr culture without stimuli with the EnzyChromTM Succinate Assay Kit (BioAssay Systems, Hayward, CA), as described[11]. The assay sensitivity was 12 μM and the intra- and interassay co-efficient of variances were less than 3.5 and 6.95%, respectively. Succinate intracellular levels were measured with the Succinate Colorimetric Assay kit (Sigma).

Gene expression analysis

Total RNA was extracted from tissues/cells using the RNeasy Lipid Tissue Mini Kit (Qiagen Science, Hilden, Germany). Total RNA quantity was measured at 260 nm and purity was assessed by the OD260/OD280 ratio. One microgram of RNA was transcribed to cDNA with random primers using the Reverse Transcription System (Applied Biosystems, Foster City, CA, USA). Quantitative gene expression was evaluated by Real-time PCR (qPCR) on a 7900HT Fast Real-Time PCR System using the TaqMan® Gene Expression Assay (Applied Biosystems) (Supplementary Table 4). Results were calculated using the comparative Ct method ($2^{-\Delta\Delta Ct}$), and expressed relative to the expression of the housekeeping gene 18S for human samples, and beta-2-microglobulin (B2M) for murine samples.

Microarray analyses

RNA isolation, library preparation and amplification from *Sucnr1*$^{fl/fl}$ and *LysM-Sucnr1*$^{fl/fl}$ ATMs from sc and vWAT were performed as described[58]**.** 8 μg of cDNA was subsequently fragmented, labelled and hybridised to MG-430 PM array strip (Thermo Fisher Scientific, Affymetrix, Ref; 901570). Processing of microarray samples was carried out using packages affy[59] and affyplm[60] from Bioconductor. Raw cell files were normalized using RMA background correction and summarization[61]. Technical metrics PM median, PM IQR, RMA IQR and RNA degradation described in[62] were computed and recorded as additional features for each sample. Differential expression between conditions was calculated using the moderated t-statistic by empirical Bayes shrinkage[63]. Experiment pool and Eklund metric RMA IQR were included as adjusting variables in the model to correct for technical variability. The normalized expression matrix was adjusted by the effect of the experiment pool and RMA IQR variables. This matrix was scaled and used afterwards to generate individual gene heatmaps. The log2 fold-change information (positive change when *LysM* was higher than flox/flox and negative change

when *LysM* was lower than flox/flox) was considered to rank all genes in the genome, and gene set enrichment analysis (GSEA) was performed using the Broad Institute's implementation[64] on MSigDB Hallmark collections. Hallmark gene sets were translated to mouse homologs using Biomart[65]. Statistically enriched Hallmark gene sets were also identified using the standard hypergeometric test. Significance was defined at levels of adjusted p-value smaller than four thresholds, that is, 0.25 (+), 0.10 (*), 0.05 (**) and 0.01 (***), using the Benjamini and Hochberg (BH) multiple testing correction. Pools of four animals from each genotype (*Sucnr1*$^{fl/fl}$ or *LysM*-Cre *Sucnr1*$^{fl/fl}$) were employed to obtain each experiment.

Immunoblot analysis

Cells were lysed and homogenized in M-PER buffer containing Protease Inhibitor Cocktail, and protein concentration was determined with the BCA Protein Assay Kit (both from Pierce Biotechnology, Rockford, IL). Equal amounts of total protein were separated on SDS-PAGE gels, transferred to Immobilon membranes and blocked. Immunoblot analysis was performed through the use of polyclonal antibodies against phospho-SAPK/JNK, phospo-CREB, phospo-STAT6, phospo-PKA, STAT-6 and KLF4, from Cell Signaling Technology (Danvers, MA); polyclonal antibodies against IL-10 and a monoclonal antibody for UCP1, from Abcam (Cambridge, UK); polyclonal antibodies against SUCNR1 and GAPDH from Sigma-Aldrich and FAA from Santa Cruz Biotechnology (Santa Cruz, CA). FAA and GAPDH were used a loading controls. Immunoreactive bands were visualized with SuperSignal West Femto chemiluminescent substrate (Pierce) and images were captured using the VersaDoc imaging system and Quantity One software (Bio-Rad, Hercules, CA).

Histology

Sections of 5-μm thickness were paraffin-embedded and prepared for hematoxylin and eosin (H&E) staining or for UCP1 or F4/80 immunohistochemistry. Briefly, paraffin sections were de-paraffinized and rehydrated. For UCP1 detection, heat-induced antigen retrieval of sections was carried out using Tris-buffer solution (pH 9) or citrate (pH 6) for F4/80. Slides were blocked 1 hr in blocking buffer, incubated at 4ºC overnight with the primary rabbit anti-mouse UCP1 (Abcam) or rat anti-mouse F4/80 (BioRad) antibody, followed by incubation with a donkey anti-rabbit IgG against UCP1 (GE Healthcare, Little Chalfont, UK) or a goat anti-rat against F4/80 (Vector Laboratories, Burlingame,

CA) horseradish peroxidase-conjugated antibody for 90 min at room temperature. Slides were washed thoroughly and converslips were mounted with DPX mounting medium (Sigma). Sections were observed by microscopy on a Leica DM1000 microscope (Wetzlar, Germany) and image acquisition was performed using Leica microsystems imaging software (Wetzlar, Germany).

Sucnr1 promoter study through bioinformatic analysis

ChIP-seq sequencing data from bone marrow-derived macrophages, published by Ostuni et al.[66], were aligned to the University of California Santa Cruz (UCSC) mm9 murine genome using bowtie2 aligner software (v2.2.9)[67]. Data analysis was performed using HOMER software suite (v4.9) (http://biowhat.ucsd.edu/homer/) described in Heinz et al.[68] Each ChIP-seq experiment was normalized to a total number of 10^7 uniquely mapped tags. Aligned read files were visualized by obtaining snapshot tracks from UCSC Genome browser. In order to identify STAT6 DNA binding motifs, we obtained four sequences found in STAT6 binding sites (1000 bp surrounding STAT6 peaks) from Sucnr1 (one sequence) and known classic STAT6 targets Arginase-1 (two sequences) and Chitinase-like protein 3 (one sequence). Sequence motif obtained with MEME-ChIP v. 4.12.0 software suite[69] was interrogated to TOMTOM tool in order to evaluate similarities to known transcription factor binding motifs. MEME-ChIP P-value indicates the probability that an equal or better site would be found in a random sequence of the same length conforming to the background letter frequencies; TOMTOM P-value indicates the probability that a random motif of the same width as the target would have an optimal alignment with a match score as good or better than the target's.Tomtom estimates the p-value using a null model consisting of sampling motif columns from all the columns in the set of target motifs).

Statistical analysis

Each experiment was performed two, three or four times and pooled to carry out statistical analysis. For *in vitro* data, values are reported as mean ± SEM. Differences between groups were determined using unpaired t-test (two-tailed, 95% confidence interval), and statistical significance in body weight, GTT and ITT curves were tested by two-way

ANOVA, using GraphPad Prism 5 software. P values < 0.05 were considered significant. For clinical and anthropometrical variables the Kolmorov-Smirnov test and Shapiro-Wilk test were used to test normality of variables. Normally distributed data were expressed as mean ± SD, and for variables with no Gaussian distribution values were expressed as median (25th–75th quartiles). Statistical significance was tested by unpaired t-test (two-tailed, 95% confidence interval) or Mann-Whitney U test. To analyze the differences in nominal variables between groups, we used the $\chi 2$ test. Pearson's and Spearman's correlation coefficients (two-tailed, 95% confidence interval) with Bonferroni adjustment were used to analyze the relationship between parameters. All clinical data were analyzed using Statistical Package for the Social Sciences software, version 15 (SPSS, Chicago, IL).

Data statement

Full scans for all immunoblots and source data for Fig. 1-8 are provided in supplementary information. All other data are available from the corresponding authors upon request. All microarray data are in the GEO database with accession code GSE120121 (submitted to GEO repository).

METHODS-only REFERENCES

51. Medina-Gomez, G. *et al.* PPAR gamma 2 prevents lipotoxicity by controlling adipose tissue expandability and peripheral lipid metabolism. *PLoS Genet* **3**, e64 (2007).

52. Ceperuelo-Mallafre, V. *et al.* Adipose tissue glycogen accumulation is associated with obesity-linked inflammation in humans. *Mol Metab* **5**, 5-18 (2016).

53. Serena, C. *et al.* Obesity and Type 2 Diabetes Alters the Immune Properties of Human Adipose Derived Stem Cells. *Stem Cells* **34**, 2559-2573 (2016).

54. Maymo-Masip, E. *et al.* The rise of soluble TWEAK levels in severely obese subjects after bariatric surgery may affect adipocyte-cytokine production induced by TNFalpha. *J Clin Endocrinol Metab* **98**, E1323-1333 (2013).

55. Gilmour, J.S. *et al.* Local amplification of glucocorticoids by 11 beta-hydroxysteroid dehydrogenase type 1 promotes macrophage phagocytosis of apoptotic leukocytes. *J Immunol* **176**, 7605-7611 (2006).

56. Zhang, X., Goncalves, R. & Mosser, D.M. The isolation and characterization of murine macrophages. *Curr Protoc Immunol* **Chapter 14**, Unit 14 11 (2008).

57. Trouplin, V. *et al.* Bone marrow-derived macrophage production. *J Vis Exp*, e50966 (2013).

58. Gonzalez-Roca, E. *et al.* Accurate expression profiling of very small cell populations. *PLoS One* **5**, e14418 (2010).

59. Gautier, L., Cope, L., Bolstad, B.M. & Irizarry, R.A. affy--analysis of Affymetrix GeneChip data at the probe level. *Bioinformatics* **20**, 307-315 (2004).

60. Heber, S. & Sick, B. Quality assessment of Affymetrix GeneChip data. *OMICS* **10**, 358-368 (2006).

61. Irizarry, R.A. *et al.* Exploration, normalization, and summaries of high density oligonucleotide array probe level data. *Biostatistics* **4**, 249-264 (2003).

62. Eklund, A.C. & Szallasi, Z. Correction of technical bias in clinical microarray data improves concordance with known biological information. *Genome Biol* **9**, R26 (2008).

63. Ritchie, M.E. *et al.* limma powers differential expression analyses for RNA-sequencing and microarray studies. *Nucleic Acids Res* **43**, e47 (2015).

64. Subramanian, A. *et al.* Gene set enrichment analysis: a knowledge-based approach for interpreting genome-wide expression profiles. *Proc Natl Acad Sci U S A* **102**, 15545-15550 (2005).

65. Durinck, S., Spellman, P.T., Birney, E. & Huber, W. Mapping identifiers for the integration of genomic datasets with the R/Bioconductor package biomaRt. *Nat Protoc* **4**, 1184-1191 (2009).

66. Ostuni, R. *et al.* Latent enhancers activated by stimulation in differentiated cells. *Cell* **152**, 157-171 (2013).

67. Langmead, B. & Salzberg, S.L. Fast gapped-read alignment with Bowtie 2. *Nat Methods* **9**, 357-359 (2012).

68. Heinz, S. *et al.* Simple combinations of lineage-determining transcription factors prime cis-regulatory elements required for macrophage and B cell identities. *Mol Cell* **38**, 576-589 (2010).

69. Bailey, T.L. *et al.* MEME SUITE: tools for motif discovery and searching. *Nucleic Acids Res* **37**, W202-208 (2009).

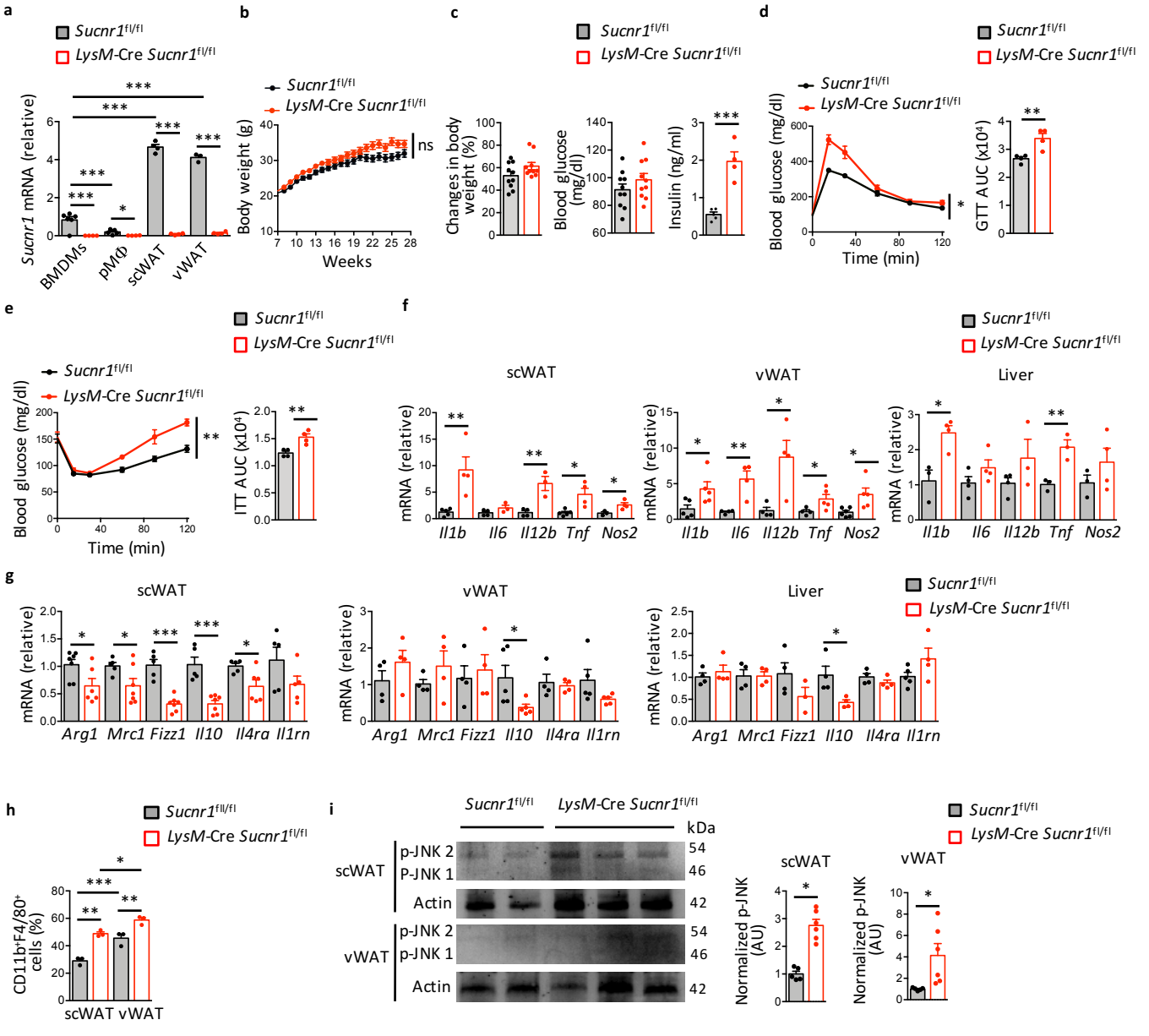
a
Sucnr1fl/fl
LysM-Cre Sucnr1fl/fl
Sucnr1 mRNA (relative)
BMDMs
pMΦ
scWAT
vWAT
b
Body weight (g)
Weeks
ns
c
Changes in body weight (%)
Blood glucose (mg/dl)
Insulin (ng/ml)
d
Blood glucose (mg/dl)
Time (min)
GTT AUC (x10⁴)
e
ITT AUC (x10⁴)
f
scWAT
vWAT
Liver
mRNA (relative)
Il1b
Il6
Il12b
Tnf
Nos2
g
Arg1
Mrc1
Fizz1
Il10
Il4ra
Il1rn
h
CD11b+F4/80+ cells (%)
i
kDa
p-JNK 2
p-JNK 1
Actin
54
46
42
Normalized p-JNK (AU)

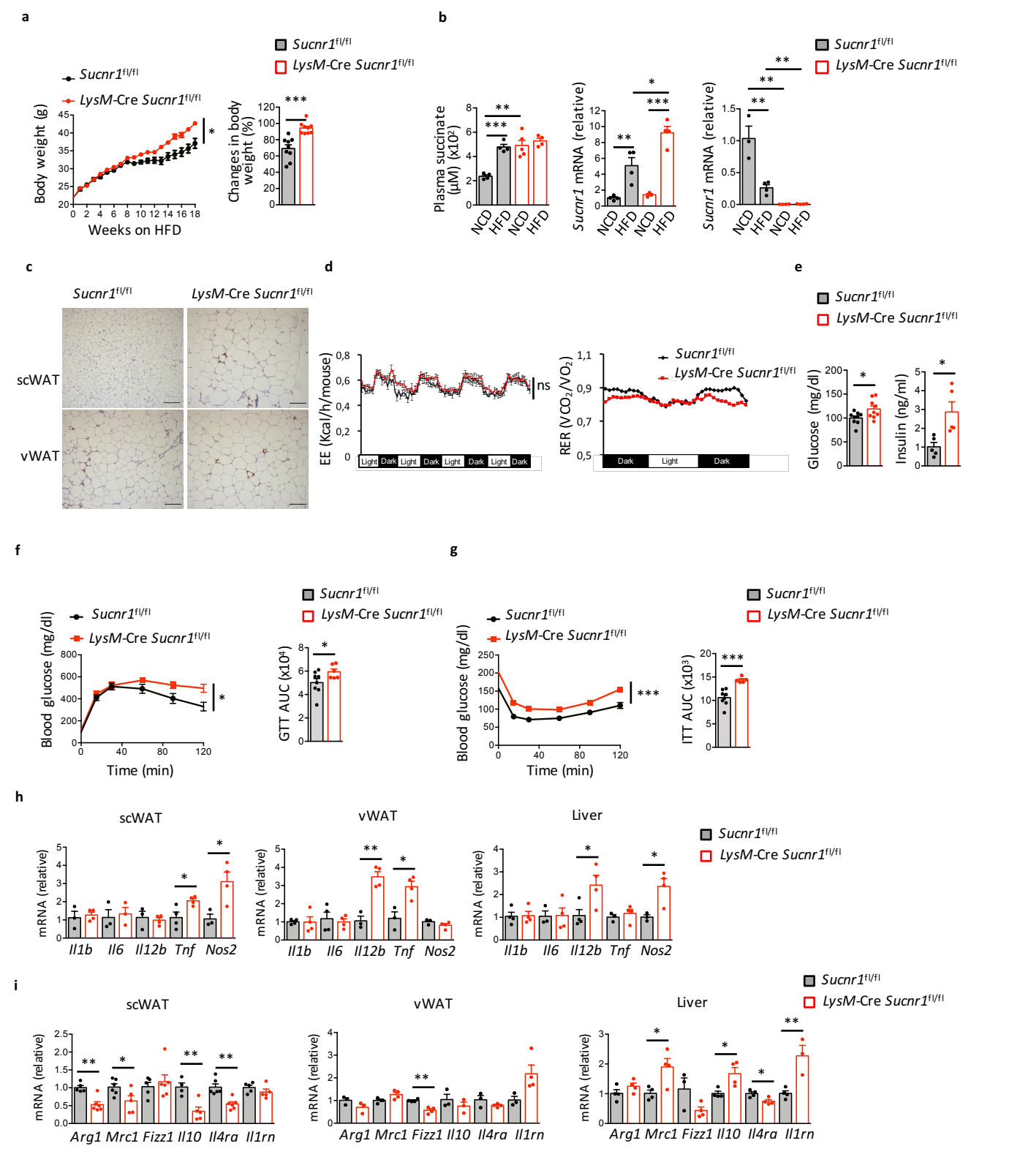
a
Sucnr1fl/fl
LysM-Cre Sucnr1fl/fl
Body weight (g)
Weeks on HFD
Changes in body weight (%)
b
Plasma succinate (μM) (x10²)
Sucnr1 mRNA (relative)
NCD
HFD
c
scWAT
vWAT
d
EE (Kcal/h/mouse)
RER (VCO2/VO2)
Light
Dark
ns
e
Glucose (mg/dl)
Insulin (ng/ml)
f
Blood glucose (mg/dl)
Time (min)
GTT AUC (x10⁴)
g
ITT AUC (x10³)
h
scWAT
vWAT
Liver
mRNA (relative)
Il1b
Il6
Il12b
Tnf
Nos2
i
Arg1
Mrc1
Fizz1
Il10
Il4ra
Il1rn

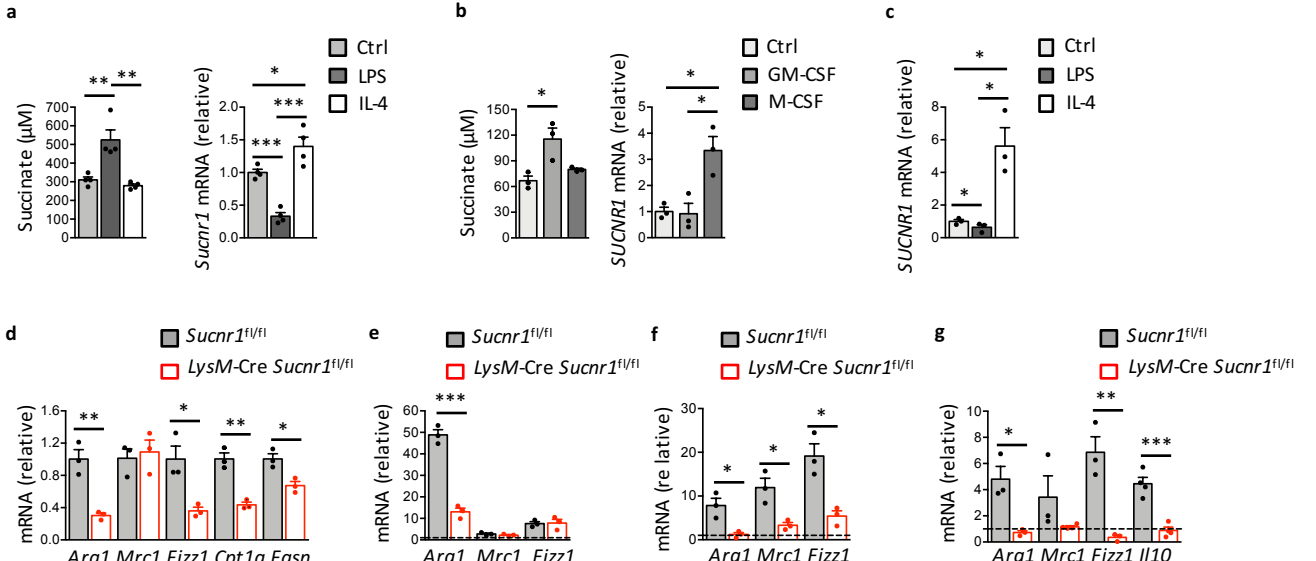
a
Succinate (μM)
Sucnr1 mRNA (relative)
Ctrl
LPS
IL-4
b
Succinate (μM)
SUCNR1 mRNA (relative)
Ctrl
GM-CSF
M-CSF
c
SUCNR1 mRNA (relative)
Ctrl
LPS
IL-4
d
Sucnr1fl/fl
LysM-Cre Sucnr1fl/fl
mRNA (relative)
Arg1 Mrc1 Fizz1 Cpt1a Fasn
e
Sucnr1fl/fl
LysM-Cre Sucnr1fl/fl
mRNA (relative)
Arg1 Mrc1 Fizz1
f
Sucnr1fl/fl
LysM-Cre Sucnr1fl/fl
mRNA (re lative)
Arg1 Mrc1 Fizz1
g
Sucnr1fl/fl
LysM-Cre Sucnr1fl/fl
mRNA (relative)
Arg1 Mrc1 Fizz1 Il10

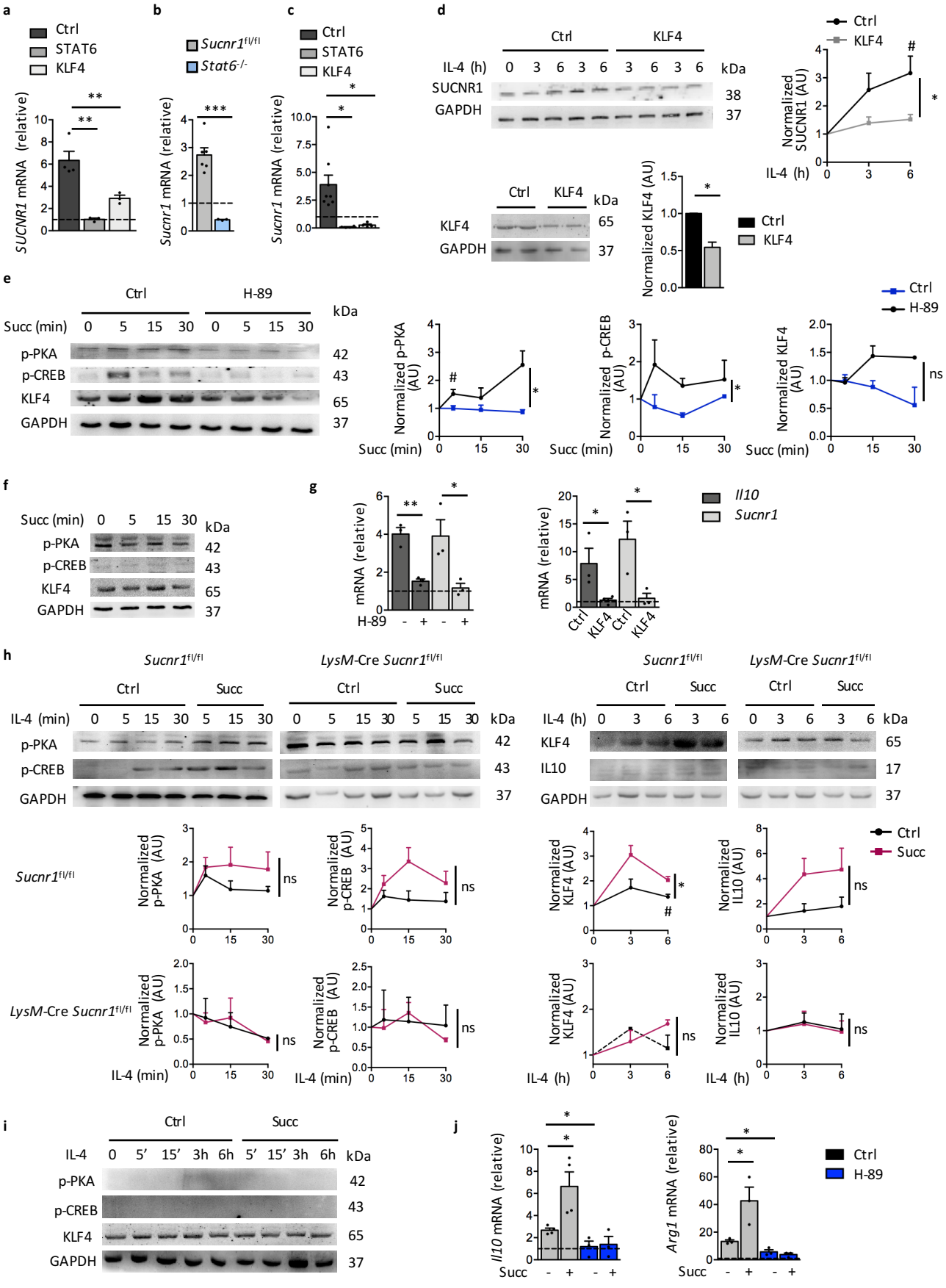
a
Ctrl
STAT6
KLF4
SUCNR1 mRNA (relative)
b
Sucnr1fl/fl
Stat6-/-
Sucnr1 mRNA (relative)
c
Ctrl
STAT6
KLF4
Sucnr1 mRNA (relative)
d
Ctrl
KLF4
IL-4 (h) 0 3 6 3 6 3 6 3 6 kDa
SUCNR1 38
GAPDH 37
Normalized SUCNR1 (AU)
IL-4 (h)
KLF4 65
GAPDH 37
Normalized KLF4 (AU)
e
Ctrl
H-89
Succ (min) 0 5 15 30 0 5 15 30 kDa
p-PKA 42
p-CREB 43
KLF4 65
GAPDH 37
Normalized p-PKA (AU)
Normalized p-CREB (AU)
Normalized KLF4 (AU)
Succ (min)
ns
f
Succ (min) 0 5 15 30 kDa
p-PKA 42
p-CREB 43
KLF4 65
GAPDH 37
g
Il10
Sucnr1
mRNA (relative)
H-89 - + - +
Ctrl KLF4 Ctrl KLF4
h
Sucnr1fl/fl
LysM-Cre Sucnr1fl/fl
Ctrl Succ Ctrl Succ
IL-4 (min) 0 5 15 30 5 15 30 0 5 15 30 5 15 30 kDa
p-PKA 42
p-CREB 43
GAPDH 37
IL-4 (h) 0 3 6 3 6 0 3 6 3 6 kDa
KLF4 65
IL10 17
GAPDH 37
Normalized p-PKA (AU)
Normalized p-CREB (AU)
Normalized KLF4 (AU)
Normalized IL10 (AU)
ns
IL-4 (min)
IL-4 (h)
i
Ctrl
Succ
IL-4 0 5′ 15′ 3h 6h 5′ 15′ 3h 6h kDa
p-PKA 42
p-CREB 43
KLF4 65
GAPDH 37
j
Il10 mRNA (relative)
Arg1 mRNA (relative)
Succ - + - +
Ctrl
H-89

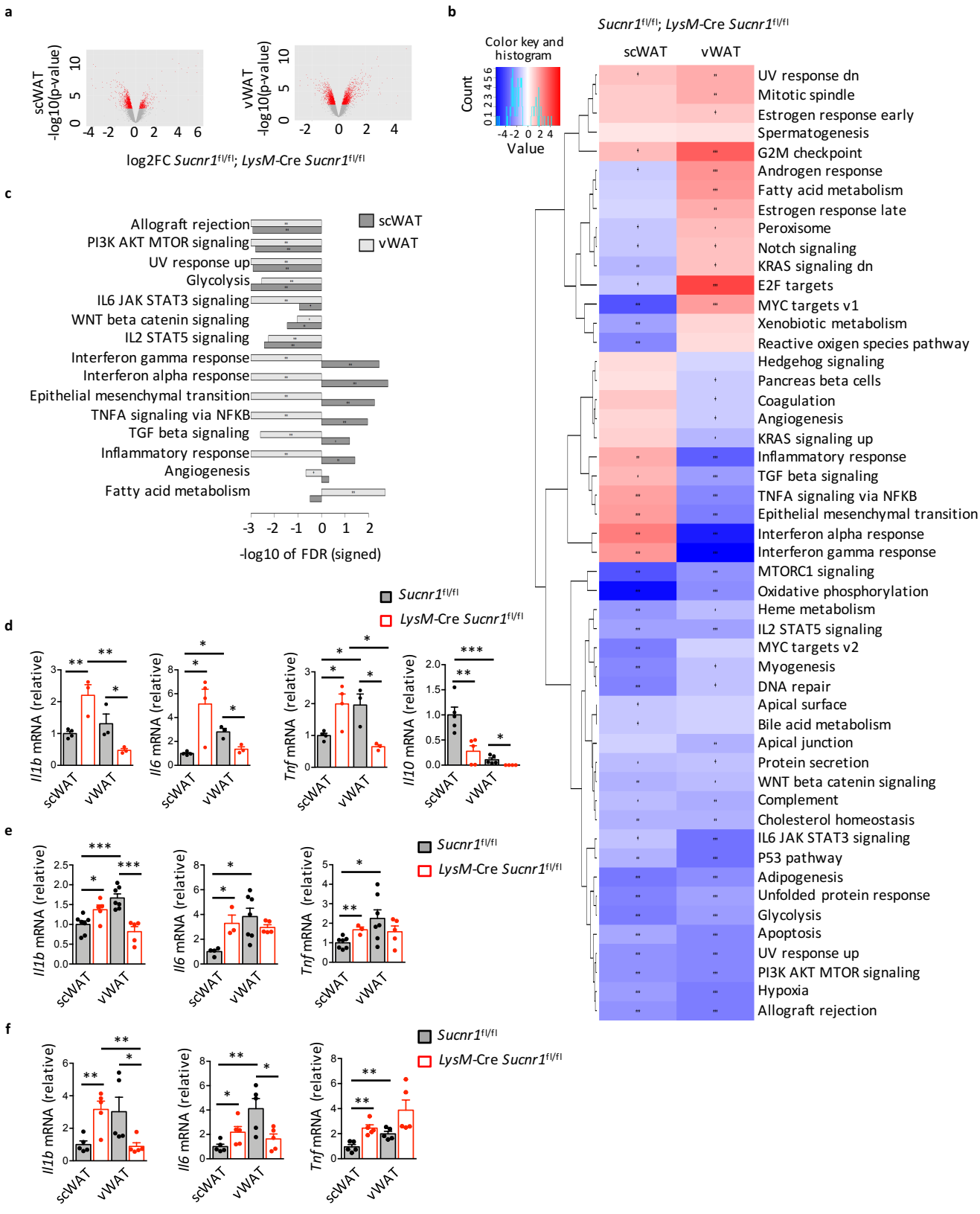
a
scWAT
-log10(p-value)
vWAT
-log10(p-value)
log2FC Sucnr1fl/fl; LysM-Cre Sucnr1fl/fl
b
Sucnr1fl/fl; LysM-Cre Sucnr1fl/fl
Color key and histogram
Count
Value
scWAT
vWAT
UV response dn
Mitotic spindle
Estrogen response early
Spermatogenesis
G2M checkpoint
Androgen response
Fatty acid metabolism
Estrogen response late
Peroxisome
Notch signaling
KRAS signaling dn
E2F targets
MYC targets v1
Xenobiotic metabolism
Reactive oxigen species pathway
Hedgehog signaling
Pancreas beta cells
Coagulation
Angiogenesis
KRAS signaling up
Inflammatory response
TGF beta signaling
TNFA signaling via NFKB
Epithelial mesenchymal transition
Interferon alpha response
Interferon gamma response
MTORC1 signaling
Oxidative phosphorylation
Heme metabolism
IL2 STAT5 signaling
MYC targets v2
Myogenesis
DNA repair
Apical surface
Bile acid metabolism
Apical junction
Protein secretion
WNT beta catenin signaling
Complement
Cholesterol homeostasis
IL6 JAK STAT3 signaling
P53 pathway
Adipogenesis
Unfolded protein response
Glycolysis
Apoptosis
UV response up
PI3K AKT MTOR signaling
Hypoxia
Allograft rejection
c
scWAT
vWAT
Allograft rejection
PI3K AKT MTOR signaling
UV response up
Glycolysis
IL6 JAK STAT3 signaling
WNT beta catenin signaling
IL2 STAT5 signaling
Interferon gamma response
Interferon alpha response
Epithelial mesenchymal transition
TNFA signaling via NFKB
TGF beta signaling
Inflammatory response
Angiogenesis
Fatty acid metabolism
-log10 of FDR (signed)
d
Sucnr1fl/fl
LysM-Cre Sucnr1fl/fl
Il1b mRNA (relative)
Il6 mRNA (relative)
Tnf mRNA (relative)
Il10 mRNA (relative)
scWAT
vWAT
e
Sucnr1fl/fl
LysM-Cre Sucnr1fl/fl
Il1b mRNA (relative)
Il6 mRNA (relative)
Tnf mRNA (relative)
scWAT
vWAT
f
Sucnr1fl/fl
LysM-Cre Sucnr1fl/fl
Il1b mRNA (relative)
Il6 mRNA (relative)
Tnf mRNA (relative)
scWAT
vWAT

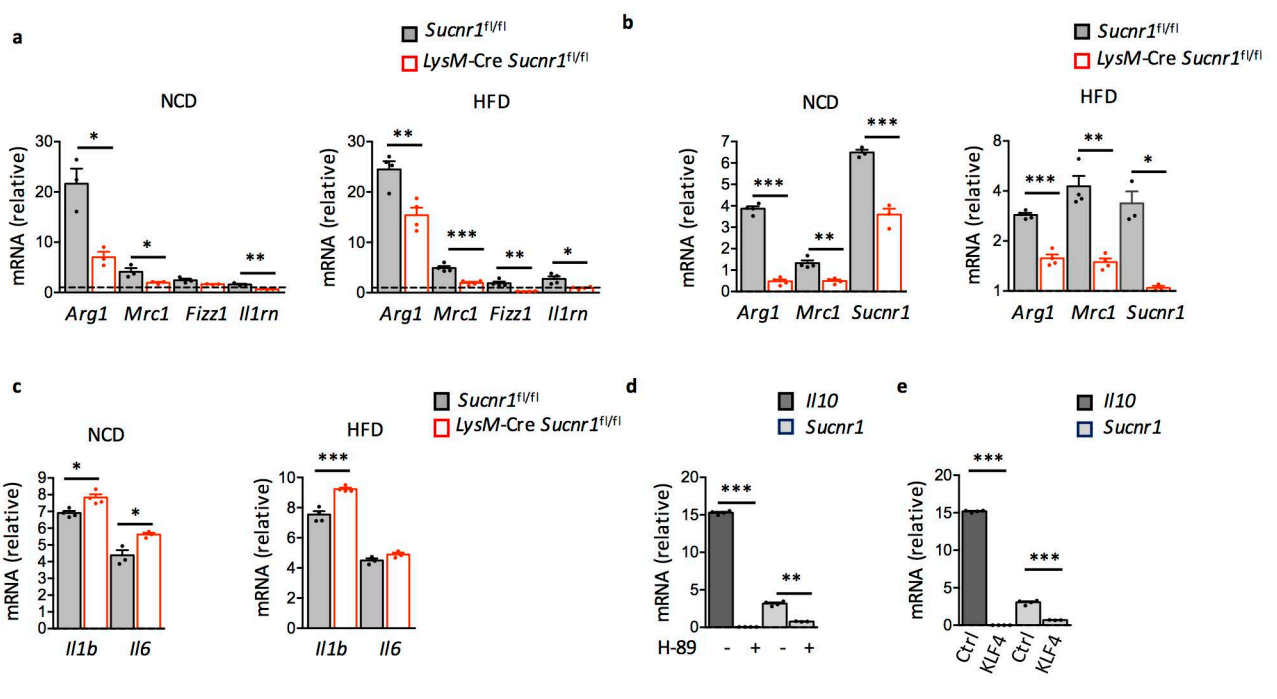
a
Sucnr1fl/fl
LysM-Cre Sucnr1fl/fl
NCD
HFD
mRNA (relative)
Arg1
Mrc1
Fizz1
Il1rn
b
Sucnr1fl/fl
LysM-Cre Sucnr1fl/fl
NCD
HFD
mRNA (relative)
Arg1
Mrc1
Sucnr1
c
Sucnr1fl/fl
LysM-Cre Sucnr1fl/fl
NCD
HFD
mRNA (relative)
Il1b
Il6
d
Il10
Sucnr1
mRNA (relative)
H-89
e
Il10
Sucnr1
mRNA (relative)
Ctrl
KLF4

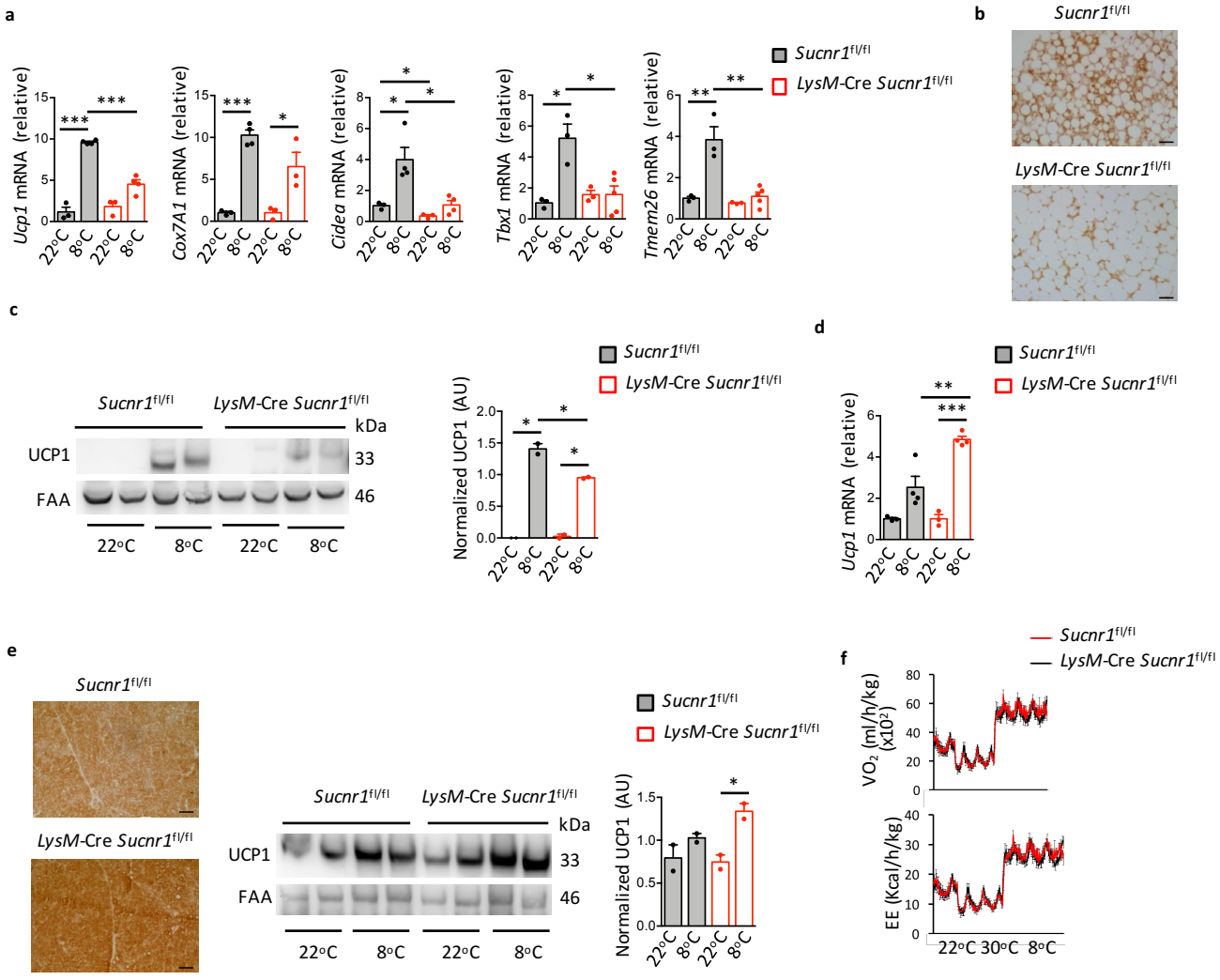
a
Ucp1 mRNA (relative)
Cox7A1 mRNA (relative)
Cidea mRNA (relative)
Tbx1 mRNA (relative)
Tmem26 mRNA (relative)
22°C
8°C
Sucnr1fl/fl
LysM-Cre Sucnr1fl/fl
b
Sucnr1fl/fl
LysM-Cre Sucnr1fl/fl
c
Sucnr1fl/fl
LysM-Cre Sucnr1fl/fl
kDa
UCP1
FAA
33
46
Normalized UCP1 (AU)
d
Ucp1 mRNA (relative)
e
Sucnr1fl/fl
LysM-Cre Sucnr1fl/fl
f
VO2 (ml/h/kg) (x10²)
EE (Kcal/h/kg)
22°C 30°C 8°C

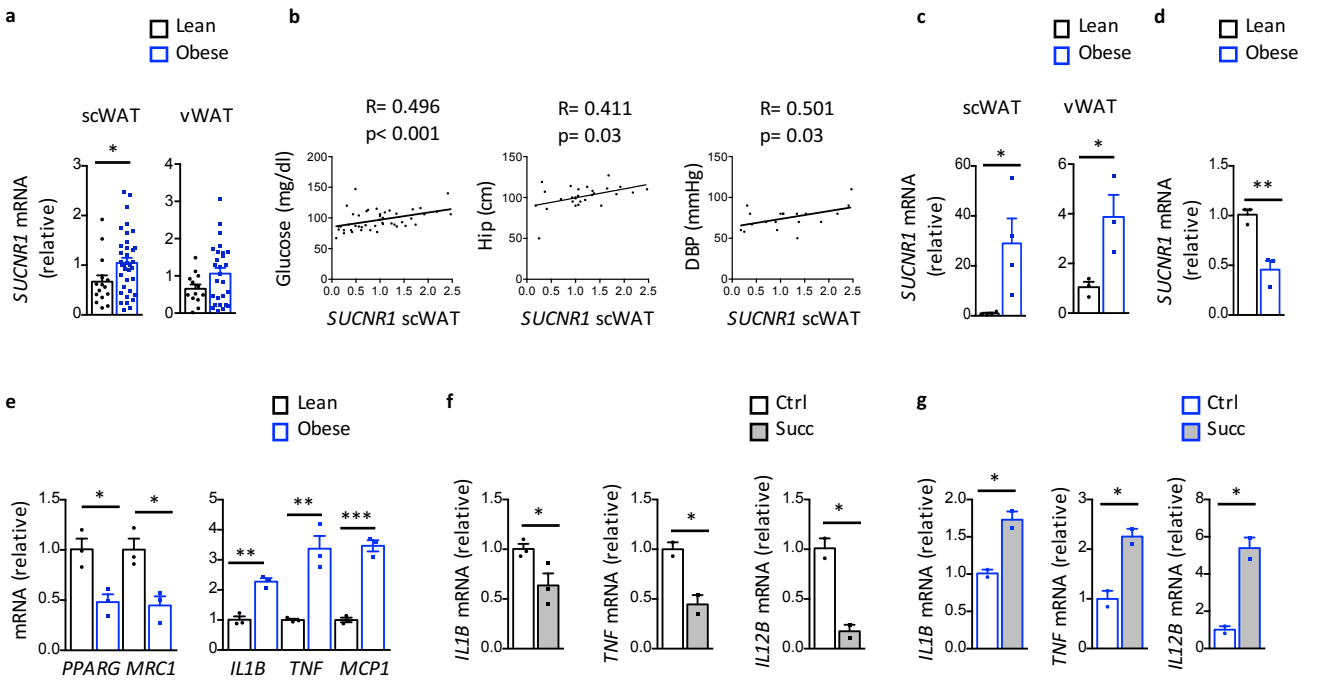
a
Lean
Obese
scWAT
vWAT
SUCNR1 mRNA (relative)
b
R= 0.496
p< 0.001
R= 0.411
p= 0.03
R= 0.501
p= 0.03
Glucose (mg/dl)
Hip (cm)
DBP (mmHg)
SUCNR1 scWAT
c
Lean
Obese
scWAT
vWAT
SUCNR1 mRNA (relative)
d
Lean
Obese
SUCNR1 mRNA (relative)
e
Lean
Obese
mRNA (relative)
PPARG
MRC1
IL1B
TNF
MCP1
f
Ctrl
Succ
IL1B mRNA (relative)
TNF mRNA (relative)
IL12B mRNA (relative)
g
Ctrl
Succ
IL1B mRNA (relative)
TNF mRNA (relative)
IL12B mRNA (relative)

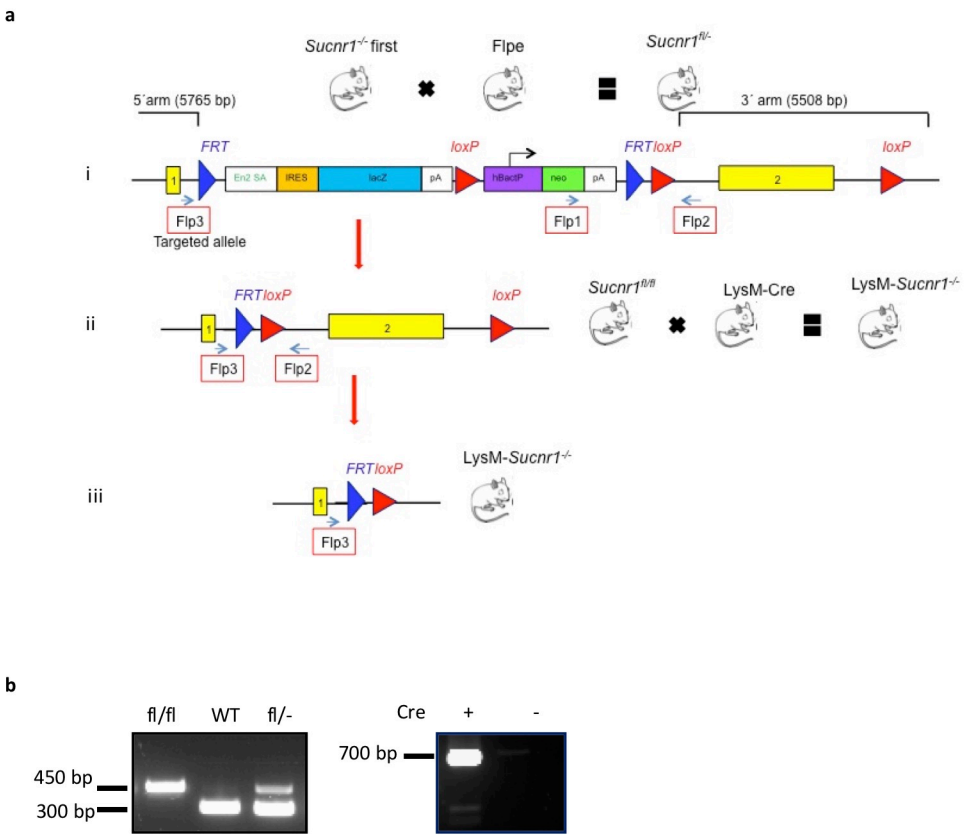

Supplementary Figure 1

Generation of myeloid-specific deletion of *Sucnr1* in mice

(**a**) Schematic diagrams showing from top to bottom, i) the structure of the targeting vector including the loxP sites (red arrowheads) on either side of exon 2 of the *Sucnr1* locus; ii) the locus after Flp-mediated recombination of the FRT sites (blue arrowheads); iii) the locus after Cre-mediated deletion of the *lox*P sites. Primers used for genotyping are shown by small arrows (Flp2 and flp3). Yellow boxes represent exons. (**b**) Representative image of systematically mice genotyping; 300bp band for wild-type (WT) allele; 450bp band for *lox*P-containing (fl/fl) allele (left); and 700bp band for the presence of Cre-recombinase gene in mice (right).

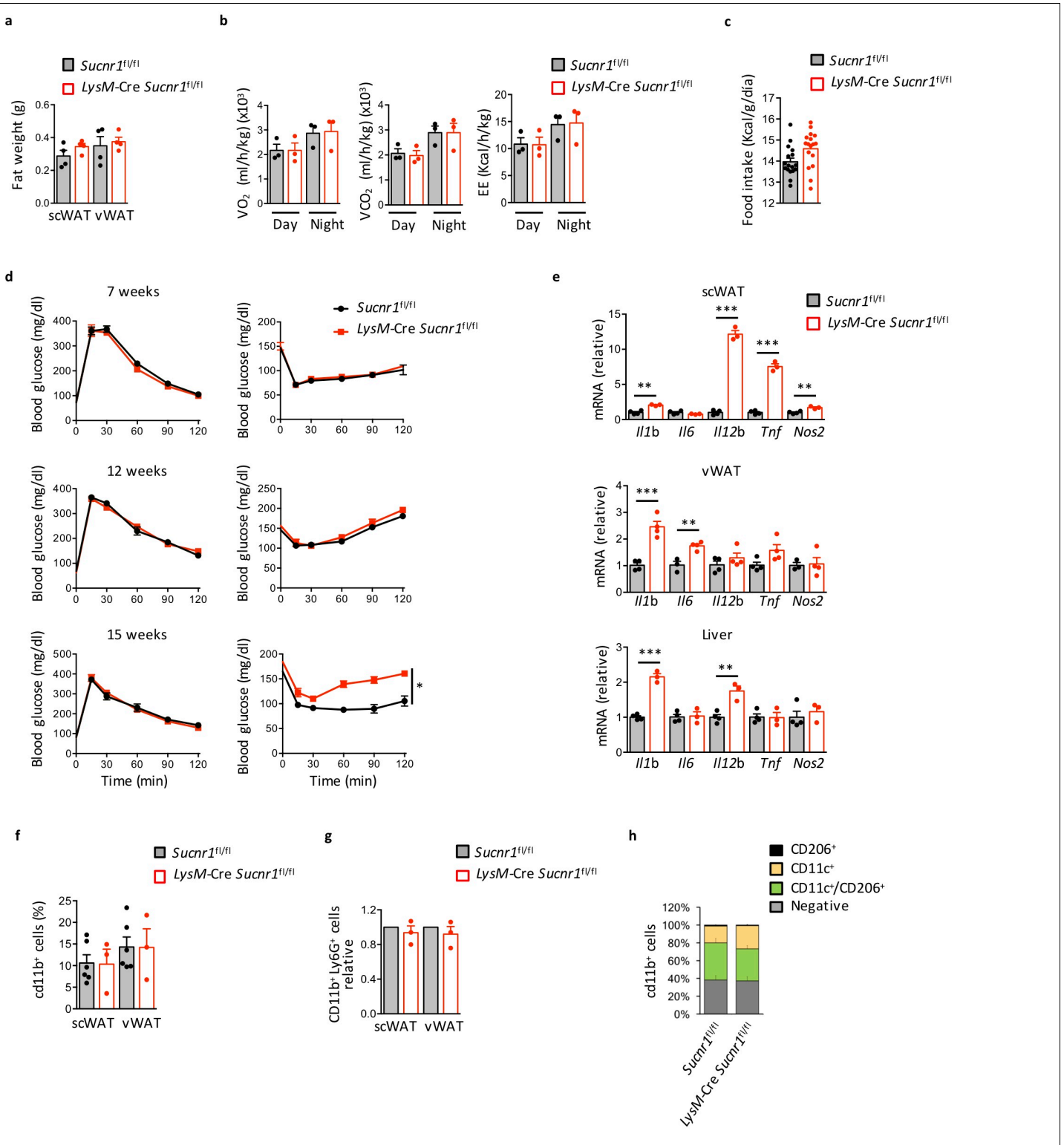

Supplementary Figure 2

***LysM*-Cre *Sucnr1*$^{fl/fl}$ mice fed a normal chow diet (NCD) develop an inflammatory profile that precedes insulin resistance**

(**a**) Fat weight of subcutaneous (sc) and visceral (v) white adipose tissue (WAT) from *LysM*-Cre *Sucnr1*$^{fl/fl}$ mice and age-matched control (*Sucnr1*$^{fl/fl}$) littermates fed a NCD (n=4 mice). (**b**) Oxygen consumption (VO_2), carbon dioxide (VCO_2) production and energy expenditure (EE), for 3 days (n=3). (**c**) Food intake as in (**a**) from two independent experiments (n=10 mice). (**d**) Glucose-tolerance test (GTT) (left) and insulin-tolerance test (ITT) (right) from top to bottom at 7 (n=6 mice for GTT and n=5 for ITT), 12 weeks (n=5 mice) and 15 weeks (n=5 for *Sucnr1*$^{fl/fl}$ and n=7 or 6 for GTT and ITT respectively, for *LysM*-Cre *Sucnr1*$^{fl/fl}$ mice) of age. (**e**) qPCR analysis of selected pro-inflammatory markers in sc and vWAT and liver from mice as in (**a**) (n=4 mice). (**f**) CD11b^{+} cells from total sc and vWAT stromal vascular fraction (SVF) of mice as in (**a**), expressed in percentages (n=6 for *Sucnr1*$^{fl/fl}$ or 3 for *LysM*-Cre *Sucnr1*$^{fl/fl}$ biologically independent samples). **(g-h)** Flow cytometry analyses of (**g**) CD11b^{+}/Ly6G^{+} population from SVF as in (**f**) (n=3) biologically independent samples, positive cells are quantified and presented relative to the *Sucnr1*$^{fl/fl}$ group set as 1 and of (**h**) CD11b^{+}/CD11c^{+} and CD11b^{+}/CD206^{+} population in SVF of scWAT as in (**f**). Amounts of CD11c+, CD206+ or CD11c+/CD206+ population are quantified and presented as relative percentage over the total number of cells analyzed (n=3 biologically independent samples). All data are shown as mean ± SEM; *P < 0.05; **P < 0.01; ***P < 0.001 (two-tailed unpaired t-test in bar graphs and two-way ANOVA in GTT and ITT curves).

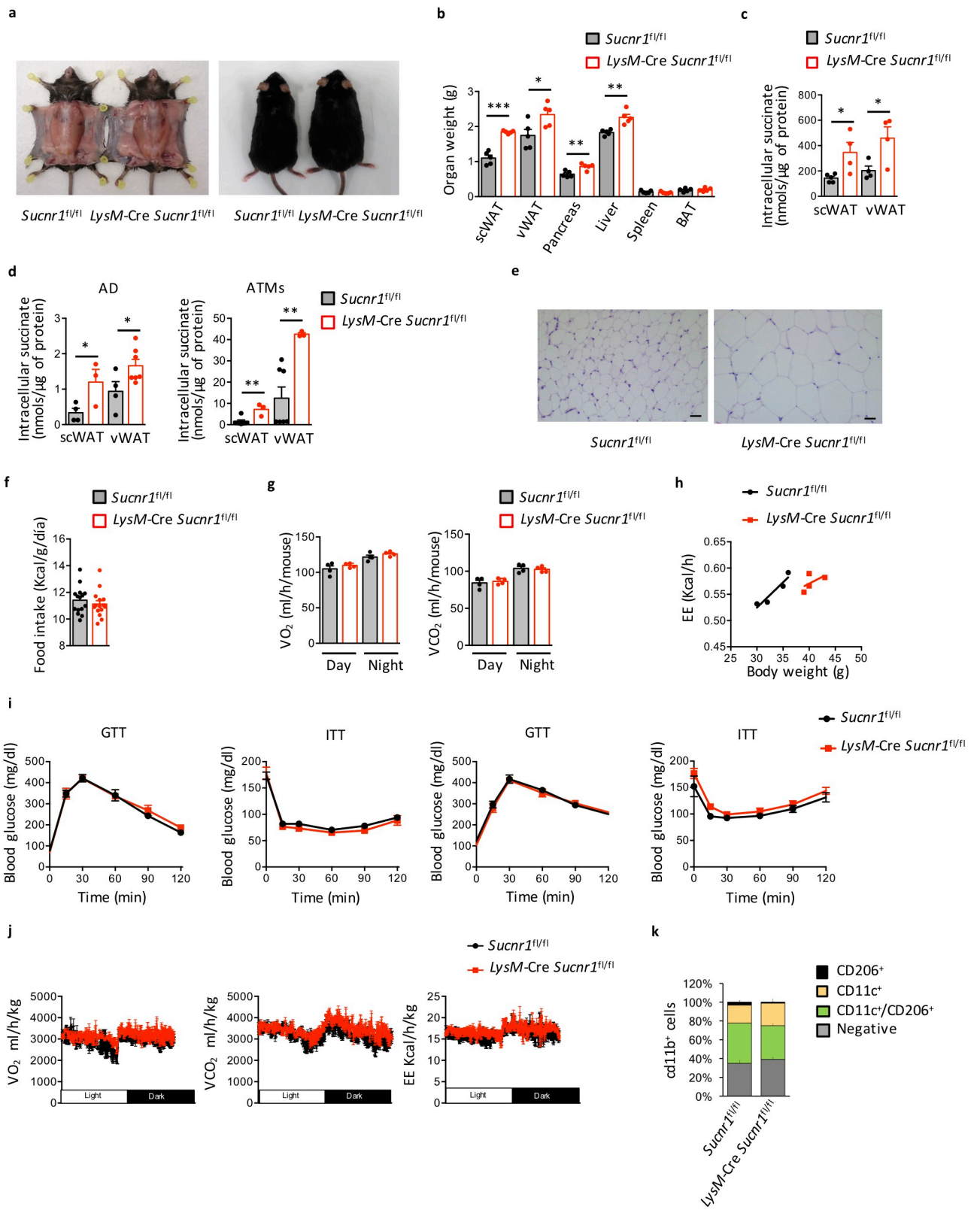

Supplementary Figure 3

Inflammatory profile associated with *LysM*-Cre *Sucnr1*$^{fl/fl}$ mice fed a high fat diet (HFD) is accompanied by an increase in fat depot mass and intracellular succinate accumulation

(**a-k**) Male *LysM*-Cre *Sucnr1*$^{fl/fl}$ mice and age-matched *Sucnr1*$^{fl/fl}$ littermates were fed a HFD. (**a**) Representative images of mouse size and scWAT depot content. (**b**) Organ weight (n=5 mice). (**c-d**) Intracellular succinate levels in (**c**) sc and vWAT (n=4 mice except n=5 for *Sucnr1*$^{fl/fl}$ scWAT) (**d**) adipocytes (AD) (n=4 for *Sucnr1*$^{fl/fl}$ and n=3 or 7 for *LysM*-Cre *Sucnr1*$^{fl/fl}$ scWAT and vWAT respectively) and adipose tissue macrophages (ATMs) (n=6 or 7 for *Sucnr1*$^{fl/fl}$ scWAT and vWAT respectively and n=3 for *LysM*-Cre *Sucnr1*$^{fl/fl}$ from biologically independent samples). (**e**) Hematoxylin and eosin (H&E) staining of scWAT sections, representative images from two independent experiments (n=4 mice). Scale bars 200 μm. (**f**) Food intake from two independent experiments (n=9 mice), (**g**) VO_2 consumption, VCO_2 production for 4 days (n=4 mice) and (**h**) analysis of EE vs body weight of ANCOVA (n=4 mice). (**i**) GTT and ITT at 11 (left) or 15 weeks of age (right) (n=5 mice except n=7 for GTT at 15 weeks). (**j**) VO_2 consumption, VCO_2 production and EE for a period of 24 hr, before differences in body weight after 7 weeks on HFD (n=5 mice). (**k**) Flow cytometry analyses of $CD11b^+/CD11c^+$ and $CD11b^+/CD206^+$ population in SVF of scWAT. Amounts of $CD11c^+$, $CD206^+$ or $CD11c^+/CD206^+$ are quantified and presented as relative percentage over the total number of cells analysed, (n=2 biologically independent samples). All data are shown as mean ± SEM; *P < 0.05; **P < 0.01; ***P < 0.001 (two-tailed unpaired t-test in bar graphs and two-way ANOVA in GTT and ITT curves).

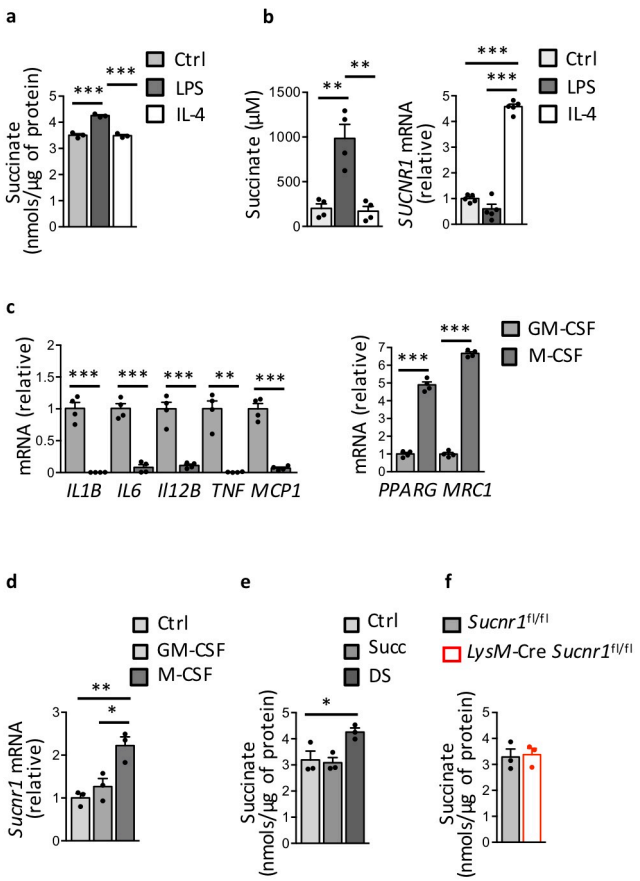

Supplementary Figure 4

SUCNR1 is predominantly expressed in anti-inflammatory macrophages and intra- and extracellular accumulation of succinate is associated with a pro-inflammatory phenotype

(**a**) Intracellular succinate levels in peritoneal macrophages from *Sucnr1*$^{fl/fl}$ mice without stimulation (ctrl) and stimulated with LPS or recombinant human IL-4 for 6 hr (n=3 biologically independent samples). (**b**) Succinate secretion in 24 hr conditioned medium (left) (n=4 biologically independent samples) and expression of *SUCNR1* (right) (n=5 biologically independent samples) in THP1 cells without stimulation (ctrl) and stimulated with LPS or recombinant human IL-4 for 6 hr. (**c**) qPCR analysis of expression of typical pro-inflammatory (left) and anti-inflammatory (right) markers from hPBMCs macrophages (BMI 22.87±1.51) obtained by treatment with GM-CSF or M-CSF for 7 d (n=4 biologically independent samples). (**d**) qPCR analysis of expression of *Sucnr1* in BMDMs unstimulated (ctrl) or stimulated with GM-CSF or M-CSF for 7 d (n=3 biologically independent samples). (**e-f**) Intracellular succinate levels in BMDMs stimulated with M-CSF for 7 d from (**e**) *Sucnr1*$^{fl/fl}$ mice without treatment (ctrl) or stimulated with succinate (Succ) or dimethyl succinate (DS) for 1 hr and from (**f**) *Sucnr1*$^{fl/fl}$ vs *LysM*-Cre Sucnr1$^{fl/fl}$ mice (n=3 biologically independent samples). Values are expressed as mean ± SEM; *P < 0.05; **P < 0.01; ***P < 0.001 (two-tailed unpaired t-test).

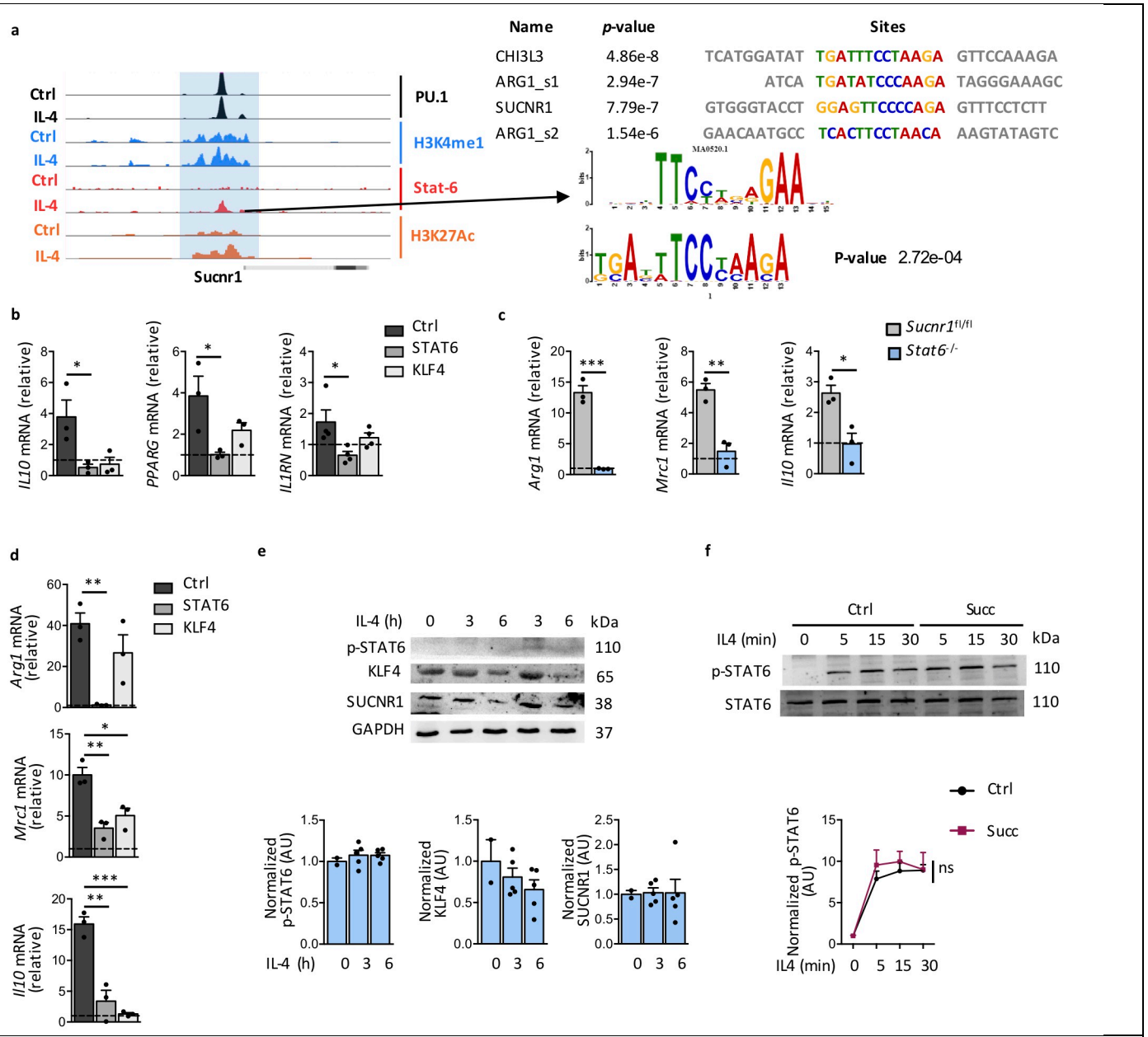

Supplementary Figure 5

SUCNR1 expression is dependent on IL-4 signaling through KLF4

(**a**) Distribution of PU.1, H3K4me1, Stat6 and H3K27Ac tag densities in the vicinity of the *Sucnr1* promoter in WT BMDMs untreated or treated for 2 hr with IL-4. Data were obtained from GEO public database with accession number GSE38377 (left). Motif analysis obtained from IL-4 stimulation for 2 hr, showing ChIP-seq dataset GSE72964, in which Stat6 peak was found in the promoter region, using web based MEME suite software (right). A motif logo representation (lower logo) as the best known motif matched, based on predictive *P*-value was obtained using TOMTOM from MEME software suit (Upper logo represents consensus sequence from JASPAR database). (**b-c**) qPCR analysis in (**b**) THP1 cells transfected with siRNAs against *STAT6*, *KLF4* or ctrl and stimulated with human IL-4 for 6 hr (n=3 except for *IL1RN* n=4 biologically independent samples) and in (**c**) BMDMs stimulated with M-CSF followed by IL-4 stimulation for 6 hr from *Sucnr1*$^{fl/fl}$ and *Stat6*$^{-/-}$ mice (n=3 biologically independent samples). (**d**) qPCR analysis from BMDMs as in (**c**) from *Sucnr1*$^{fl/fl}$ mice transfected as in (**b**), before IL-4 treatment (n=3 biologically independent samples). Results are presented relative to their respective basal state as 1 (without IL-4) for **b-d**. (**e-f**) Representative images of immunoblot analysis and densitometric analysis in arbitrary units (AU) in (**e**) BMDMs from *Stat6*$^{-/-}$ mice (n=2 independent experiments) and in (**f**) BMDMs stimulated with M-CSF from *Sucnr1*$^{fl/fl}$ mice (n=3

independent experiments). Uncropped blots are provided in source data. Values are expressed as mean ± SEM; *P < 0.05; **P < 0.01; ***P < 0.001; ns: non-significant (two-tailed unpaired t-test).

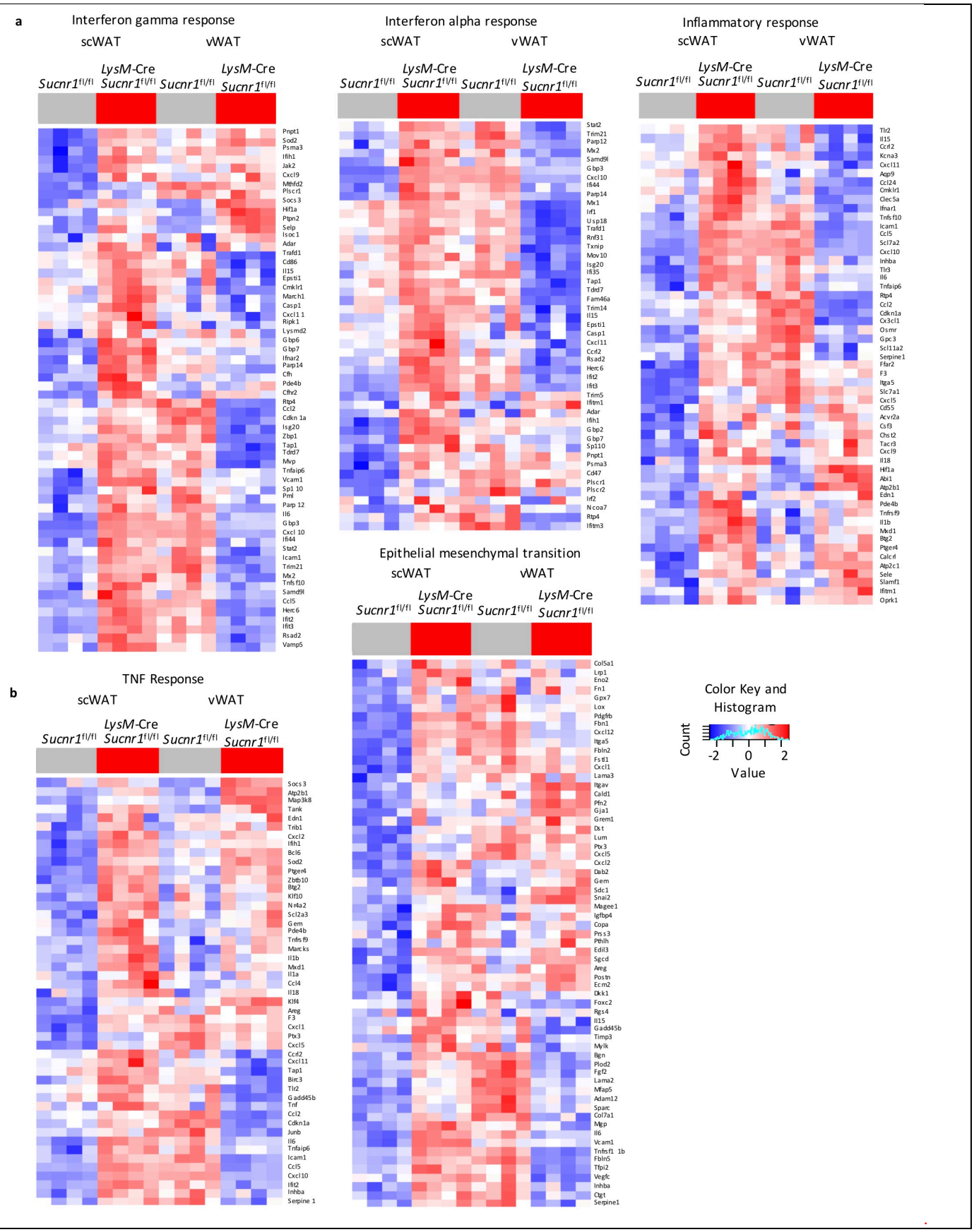
a
Interferon gamma response
scWAT
vWAT
Sucnr1fl/fl
LysM-Cre Sucnr1fl/fl
Pnpt1
Sod2
Psma3
Ifih1
Jak2
Cxcl9
Mthfd2
Plscr1
Socs 3
Hif1a
Ptpn2
Selp
Isoc1
Adar
Trafd1
Cd86
Il15
Epsti1
Cmklr1
March1
Casp1
Cxcl1 1
Ripk1
Lysmd2
Gbp6
Gbp7
Ifnar2
Parp14
Cfh
Pde4b
Cfhr2
Rtp4
Ccl2
Cdkn 1a
Isg20
Zbp1
Tap1
Tdrd7
Mvp
Tnfaip6
Vcam1
Sp1 10
Pml
Parp 12
Il6
Gbp3
Cxcl 10
Ifi44
Stat2
Icam1
Trim21
Mx2
Tnfs f10
Samd9l
Ccl5
Herc 6
Ifit2
Ifit3
Rsad2
Vamp5
Interferon alpha response
scWAT
vWAT
Stat2
Trim21
Parp12
Mx2
Samd9l
Gbp3
Cxcl10
Ifi44
Parp14
Mx1
Ifi1
Usp18
Trafd1
Rnf31
Txnip
Mov10
Isg20
Ifi35
Tap1
Tdrd7
Fam46a
Trim14
Il15
Epsti1
Casp1
Cxcl11
Ccrl2
Rsad2
Herc 6
Ifit2
Ifit3
Trim5
Ifitm1
Adar
Ifih1
Gbp2
Gbp7
Sp110
Pnpt1
Psma3
Cd47
Plscr1
Plscr2
Irf2
Ncoa7
Rtp4
Ifitm3
Inflammatory response
scWAT
vWAT
Tlr2
Il15
Ccrl2
Kcna3
Cxcl11
Aqp9
Ccl24
Cmklr1
Clec5a
Ifnar1
Tnfs f10
Icam1
Ccl5
Scl7a2
Cxcl10
Inhba
Tlr3
Il6
Tnfaip6
Rtp4
Ccl2
Cdkn1a
Cx3cl1
Osmr
Gpc3
Scl11a2
Serpine1
Ffar2
F3
Itga5
Slc7a1
Cxcl5
Cd55
Acvr2a
Csf3
Chst2
Tacr3
Cxcl9
Il18
Hif1a
Abi1
Atp2b1
Edn1
Pde4b
Tnfrs f9
Il1b
Mxd1
Btg2
Ptger4
Calcrl
Atp2c1
Sele
Slamf1
Ifitm1
Oprk1
Epithelial mesenchymal transition
scWAT
vWAT
Col5a1
Lrp1
Eno2
Fn1
Gpx7
Lox
Pdgfrb
Fbn1
Cxcl12
Itga5
Fbln2
Fstl1
Cxcl1
Lama3
Itgav
Cald1
Pfn2
Gja1
Grem1
Dst
Lum
Ptx3
Cxcl5
Cxcl2
Dab2
Gem
Sdc1
Snai2
Magee1
Igfbp4
Copa
Psrs 3
Pthlh
Edil3
Sgcd
Areg
Postn
Ecm2
Dkk1
Foxc2
Rgs4
Il15
Gadd45b
Timp3
Mylk
Bgn
Plod2
Fgf2
Lama2
Mfap5
Adam12
Sparc
Col7a1
Mgp
Il6
Vcam1
Tnfsf1 1b
Fbln5
Tfpi2
Vegfc
Inhba
Ctgt
Serpine1
b
TNF Response
scWAT
vWAT
Socs 3
Atp2b1
Map3k8
Tank
Edn1
Tnfb1
Cxcl2
Ifih1
Bcl6
Sod2
Ptger4
Zbtb10
Btg2
Klf10
Nr4a2
Scl2a3
Gem
Pde4b
Tnfrs f9
Marcks
Il1b
Mxd1
Il1a
Ccl4
Il18
Klf4
Areg
F3
Cxcl1
Ptx3
Cxcl5
Ccrl2
Cxcl11
Tap1
Birc3
Tlr2
Gadd45b
Tnf
Ccl2
Cdkn1a
Junb
Il6
Tnfaip6
Icam1
Ccl5
Cxcl10
Ifit2
Inhba
Serpine 1
Color Key and Histogram
Count
-2
0
2
Value

Supplementary Figure 6

***Sucnr1* deficiency alters the transcriptional signature of ATMs in a depot-specific manner**

(**a-b**). Heatmap with GSEA normalized enrichment scores of gene expression profile for microarray of ATMs from *LysM*-Cre *Sucnr1*$^{fl/fl}$ and *Sucnr1*$^{fl/fl}$ mice from scWAT and vWAT in the pathway of (**a**) Interferon gamma, Interferon alpha and Inflammatory response and (**b**) TNF response and Epithelial mesenchymal transition gene sets from Hallmark. Data are from n=4 biologically independent samples.

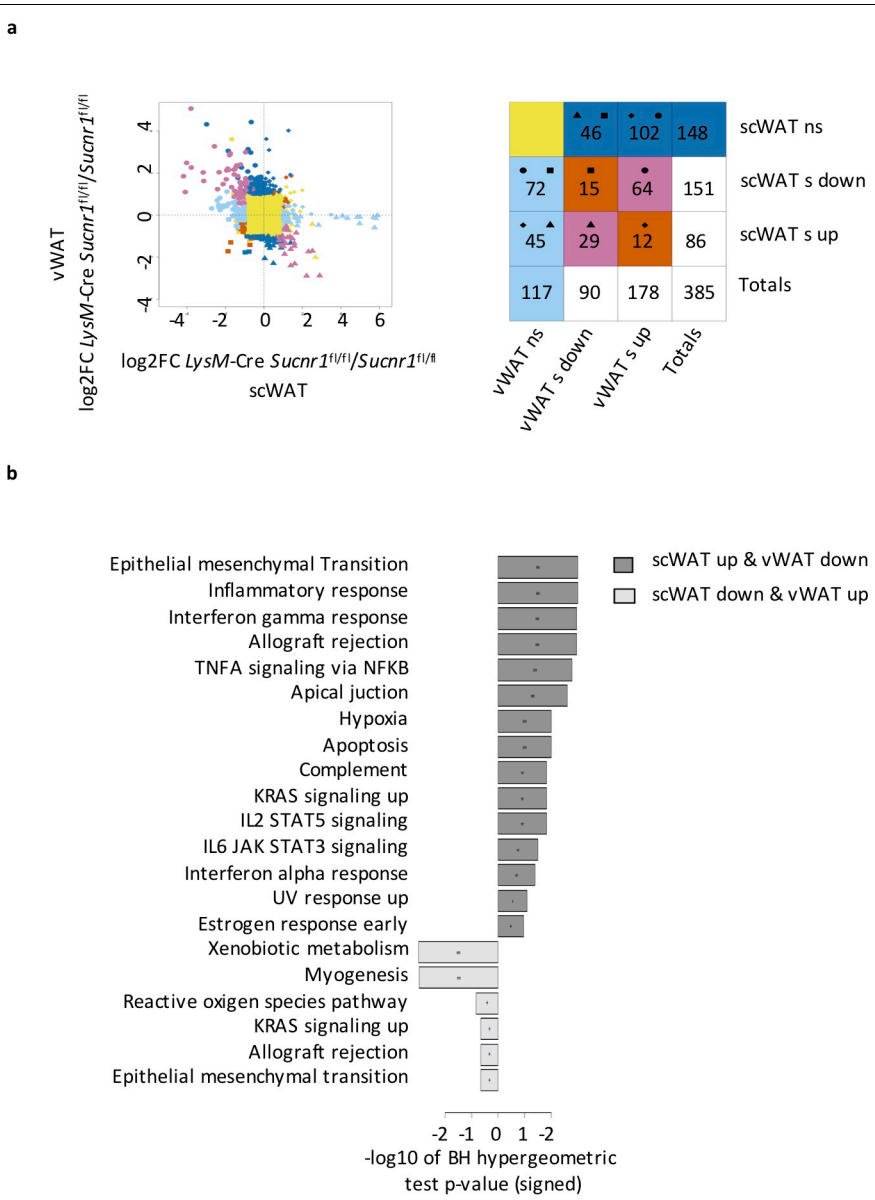

Supplementary Figure 7

GSEA analysis of the genes differentially regulated between scWAT and vWAT

(a,b) Microarrays analysis of sc and vWAT ATMs from *LysM*-Cre *Sucnr1*$^{fl/fl}$ and *Sucnr1*$^{fl/fl}$ mice. (**a**) Log_2FC in scWAT (x-axis) vs vWAT (y-axis) ATMs: top left quadrants (circles) are genes expressed higher in *LysM*-Cre *Sucnr1*$^{fl/fl}$ than in *Sucnr1*$^{fl/fl}$ for vWAT ATMs and lower in *LysM*-Cre *Sucnr1*$^{fl/fl}$ than in *Sucnr1*$^{fl/fl}$ for scWAT ATMs. Linear models with empirical Bayes statistic (Limma) where used for differential expression. Top right quadrants (diamonds) are genes expressed higher in *LysM*-Cre *Sucnr1*$^{fl/fl}$ than in *Sucnr1*$^{fl/fl}$ for both vWAT and scWAT ATMs. Bottom left quadrants (squares) are genes expressed lower in *LysM*-Cre *Sucnr1*$^{fl/fl}$ than in *Sucnr1*$^{fl/fl}$ for both vWAT and scWAT ATMs. Bottom right quadrants (triangles) are genes expressed lower in *LysM*-Cre *Sucnr1*$^{fl/fl}$ than in *Sucnr*$^{fl/fl}$ for vWAT and higher in *LysM*-Cre *Sucnr1*$^{fl/fl}$ than in *Sucnr1*$^{fl/fl}$ for scWAT ATMs. Non-yellow points correspond to genes with an abs(log_2FC) > log(2) and adjusted p-value < 0.05 in at least one of the two comparisons: orange and pink points distinguish between differentially expressed genes that go in the same direction (orange) for vWAT and scWAT ATMs and differentially expressed genes that go in opposite (pink) directions (signatures used in panel (**b**) for enrichment analysis), respectively. Differentially expressed genes for only scWAT ATMs and for only vWAT ATMs are represented in light and dark blue, respectively. Total number of genes in each of the groups is provided in the adjacent coloured table. (**b**) Hallmark gene set enrichment analysis for ATMs as in (**a**) using differentially expressed gene lists "scWAT LysM up & vWAT down" (violet-triangle in (a), shown in positive) and "scWAT LysM down & vWAT up" (pink-circle in (a), shown in negative),

(Hypergeometric test, Benjamini and Hochberg-adjusted p-values, filtered by gene sets with p-value < 0.05). Data are from n=4 biologically independent samples.